CHARACTERIZATION OF ELECTROPHORECTIC SEPARATIONS ON A CELLULOSE PAPER-MICROFLUIDIC CHIP

A Thesis

presented to

the Faculty of California Polytechnic State University,

San Luis Obispo

In Partial Fulfillment

of the Requirements for the Degree

Master of Science in Biomedical Engineering

by

Kyle Robert Fast

September 2015

COMMITTEE MEMBERSHIP

TITLE:	Characterization of Electrophoretic Separations on a Cellulose Paper-Microfluidic Chip
AUTHOR:	Kyle Robert Fast
DATE SUBMITTED:	September 2015
COMMITTEE CHAIR:	David Clague, Ph.D. Professor of Biomedical Engineering
COMMITTEE MEMBER:	Scott Hazelwood, Ph.D. Professor of Biomedical Engineering
COMMITTEE MEMBER:	Richard Savage, Ph.D. Professor of Biomedical Engineering

ABSTRACT

Characterization of Electrophoretic Separations on a Cellulose Paper-Microfluidic Chip

Kyle Robert Fast

The purpose of this thesis project is to demonstrate the ability to utilize electrophoresis in a cellulose paper microfluidic chip to manipulate charged particles. Materials were selected and a manufacturing protocol was created to successfully apply the electric field onto the paper chip. Experiments were performed to characterize the separation rates for charged, colorimetric dye, Orange G in the membrane as a function of an applied electric field, dye concentration, and distance traveled. The experiments confirmed that the electric field can be applied to the chip and particle separation rates were characterized. Next, the determined rates results were used to design a device that used a transverse electric field to the flow direction to separate Orange G into a collection channel. Results showed that electrophoresis can be used to separate the flow of charged particles on a paper microfluidic device. In conclusion, the application of electrophoresis was shown to be successful. An approach to be utilized as a sample treatment to improve the detecting capability of low cost paper devices for a more accurate diagnostic test in the developing world.

ACKNOWLEDGMENTS

Dr. David Clague

Nicole Peretti

Linda Mayo

Tim Fast

Shelly Rue

TABLE OF CONTENTS

Page

LIST OF TABLES

LIST OF FIGURES

LIST OF VARIABLES

a	Particle radius
MW	Molecular Weight
ρ	Density
N_A	Avogadro's number
δ_c	Channel Distance
δ_T	Transverse Distance
a_f	Fiber Diameter
$\propto$	Brinkman's Screening Length
t_L	Longitudinal Flow time
q	Charge
V_t	Voltage
E_x	Electric Field
ξ	Hydrodynamic Resistance
u_E	Drift Velocity
μ	Viscosity
a_f	Fiber radius
microPAD	Paper Microfluidic Device
TMD	Traditional Microfluidics paper microfluidic devices
LFA	Lateral flow assay
CDC	Center for Disease Control
EO-Flow	Electroosmotic Flow
Eph	Electrophoresis
CE	Capillary Electrophorese

CHAPTER 1: **INTRODUCTION**

Developing countries have a strong need for low cost and low power requirement diagnostic tools to improve health care. Current, traditional microfluidic devices (TMD) have been shown to detect an immense spectrum of targets, especially with the application of electrophoretic flow. However, the price and power requirements of TMDs do not allow wide use of these devices in developing countries. In an attempt to provide a low cost alternative, paper microfluidic devices (microPADs) have been created[1]. MicroPADs that are currently available have been shown to be effective in detecting a growing range of pathogens and markers, however, they still lack the functionality and specificity that has been shown in TMDs. One such modification to improve the functionality of these devices is to integrate electrophoretic separations.

When deploying a diagnostic microPAD, the device must test for its targets in a timely, reliable manner and provide accurate and reproducible results [1]. Incorporation of electrophoretic separations, or the induced movement of charged particles in an electric field, into microPADs has the potential to improve their performance. To incorporate electrophoretic flow into microPADs, redesigning of current devices is necessary.

1.1 Thesis Purpose and Objectives

1.1.1 Thesis Purpose

Based on previously published work on microPADs as a diagnostic tool [1-3], work on TMDs, and the application of electrophoretic separations and electrophoreses, this thesis will try to combine electrophoretic separations in a low cost microPAD. The

goal is to improve the potential diagnostic abilities of microPADs by redesigning the current microPADs to include the ability to perform electrophoretic separations. The aims of this thesis are to: 1) determine if electrophoretic separations can be performed on low-cost microPADs, and 2) determine if these separations can be predicted. Successful demonstration of predictable electrophoretic separation on microPADs will provide the proof of concept needed to characterize the potential use of electrophoresis in future microPADs.

1.1.2 Thesis Objectives

The following is a summary of the specific questions pursued in this thesis:

I. Can electrophoresis be achieved on a paper-microfluidic device?

II. Can electrophoretic manipulation on these devices be predicted?

III. Is the behavior reproducible?

1.2 Motivation

Rapid response to disease outbreaks is crucial in the identification and containment of a pathogen. The Global Disease Detection division (GDD) of the Center for Disease Control and Prevention (CDC) is an international organization that is tasked with identification and control of emerging infectious diseases around the world [4]. The GDD goal is to respond within 24 hours of receiving notice of an outbreak [4]. Once the GDD has responded, depending on the country and situation, field labs will be set up to identify and contain the outbreak. This is often a difficult and time consuming task. Traditional labs require large, expensive equipment and high power requirements [5]. They also need highly trained staff to operate the lab and analyze results. The use of

inexpensive, portable, and easy-to-use diagnostic equipment could significantly reduce the complexity of these missions [5]. MicroPADs are one such technology that are easy to use and show promise to improve the detection time, and thus save lives. To expand the utility of microPADs, these devices still need greater functionality to replicate and potentially replace traditional microfluidic devices in the field.

Traditional assays, a diagnostic technique used to detect pathogens, often require bench scale equipment. Paper-based lateral flow assays (LFA) can perform many of the same functions of traditional assays while being inexpensive, easy to fabricate, and easy to use. Most LFAs use a simple, straight channel design, e.g., the home pregnancy test, and typically contain three types of membranes. Sample preparation is performed in the sample pad, the first membrane that the raw sample encounters. Pre-treatment reagents can be stored in the sample pad to modify the sample for downstream processing, however, physical filtration, owing to the porous nature of the sample pad membrane, is the primary form of separating debris. To increase the specificity of a test or to test for multiple targets, it is necessary to increase the filtering of the sample. Therefore, the purpose of this thesis is to develop a way to incorporate electric fields transverse to fluid flow to enable the separation of charged particles and enhance the sample preparation of LFAs.

The following sections of this introduction will provide the background and foundation on which this thesis is based. An introduction of the current designs and components of LFAs is provided. Background information on the two main types of assays, lateral flow immunoassay and nucleic acid lateral flow immunoassay, and their detection capabilities is also explained. It is also important to understand the various

types of diseases, conditions, and compounds that can be detected using LFAs; this is also discussed. Lastly, the theory and forces governing electrophoretic separations on LFAs are described.

1.3 Electrophoresis

Electrophoresis is the separation of charged particles in a medium with an applied electric field. Additionally, through these methods, charged species can be identified based on particle size and migration rates through the medium under the influence of an electric field, the most basic of these mediums being water. Electrophoresis was first performed with water in 1937 by Tiselius in which he used a U-shaped cylinder with electrodes on either end of the tube [6]. The cylinder was filled with a colloidal mixture, or particles smaller than 2 μm, in water and when an electric gradient was applied, the mixture would separate into bands depending on the weight and charge of each species' constituents. Researchers later developed more advanced electrophoresis techniques and expanded mediums to paper and later to gel.

1.4 Paper Electrophoresis

By 1948, over 2000 papers were published investigating electrophoresis in paper [6]. Laboratories created a number of different techniques and methods to perform paper-based electrophoresis. Using these techniques, researchers and clinicians have been able to detect various ions, amino acids, proteins, and diseases [6-9]. However, paper electrophoresis has also shown to have some drawbacks that make it difficult to achieve accurate results. Common problems with paper electrophoresis originate from the inherent joule heating. The confounding effects are rapid evaporation and band

broadening due to temperature enhanced diffusion. Many different types of platforms for paper-based electrophoresis have since been created to try to address the short comings and advance the technology. These advancements can be divided into a few categories: horizontal or vertical plane separations, high or low voltage, and sieving medium options including open, semi-open, or closed matrix [6, 8, 9].

1.4.1 Horizontal and Vertical Electrophoresis

Horizon and vertical electrophoresis pertains to the plane the electrophoretic separation occurs. In a horizontal electrophoresis the electrolyte is commonly stored in reservoirs at about the same height that the electrophoresis is performed on. The purpose of the reservoirs is to keep the matrix saturated during electrophoresis. During vertical electrophoresis the solutes moves in either only the vertical or in the vertical and horizontal directions [6]. The electric field in both vertical and horizontal devices may be applied in the same direction as capillary fluid flow or in the transverse direction. For an electric field applied in the same direction as fluid flow, a paper membrane can be placed in a reservoir, pulled up over a support structure and then placed back down into another reservoir, with both reservoirs containing opposite voltage [10]. In this case, the electric field moves particles through the paper and over an incline, against gravity, with smaller particles traveling faster than larger ones. Smaller particles travel faster than larger particles because of the greater hindrance the paper matrix fibers exert on the larger particles as the particles move through the matrix. An example of this is shown in Figure 1.1.

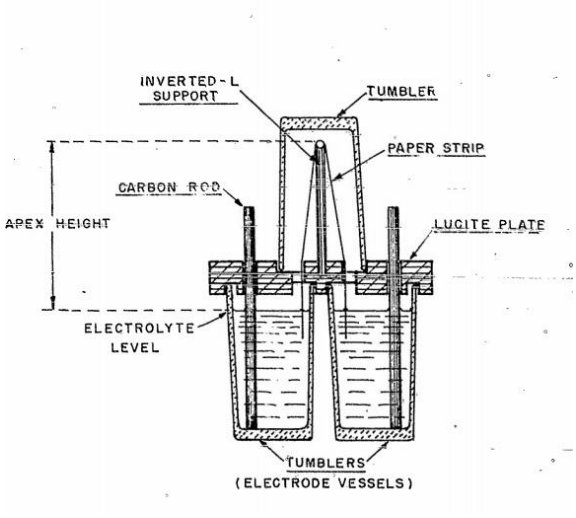

Figure 1.1 An example of a vertical paper electrophoresis device containing electrode reservoirs with paper bridging the reservoirs and suspended over a hanging bar [10].

For an electric field applied transverse to fluid flow, a paper membrane can be placed between two reservoirs, one higher than the other. In this case, electrodes are placed on either side of the paper membrane transverse to fluid flow. Fluid will then flow through due to capillary action through the paper from the top reservoir down towards the bottom reservoir with gravity as the main driving force for fluid flow, while the electric field pulls particles to either side of the paper. Separated particles can be collected individually by placing various collecting tubes at the bottom reservoir [6], see Figure 1.2. Devices of this type are also considered to be continuous because as long as the reservoir is full, the device will continue separating and filling the lower collecting tubes. The advantage to using a vertical system is that gravity prevents oversaturation and unwanted movement of particles in the filter paper, which can be a problem in a horizontal setup [6].

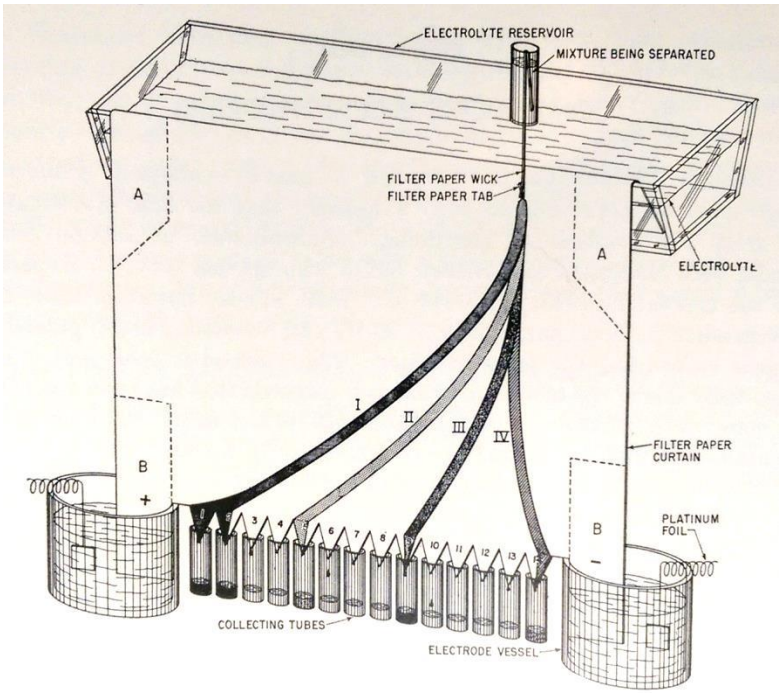

Figure 1.2 An example of vertical electrophoresis device with electric field applied transverse to fluid flow [6].

1.4.2 Open, Semi-Open, and Closed Electrophoresis

Paper electrophoresis can be also be classified by the exposure of the filter paper to the surrounding environment during the electrophoresis process. In an open setup the filter paper is exposed to the air on all sides. The open devices are usually the simplest and usually consist of a piece of filter paper draped across two reservoirs with electrodes in each reservoir. The advantages to the open set-up are the simplicity and minimal amount of equipment needed. The disadvantages, however, include a large amount of evaporation and extremely high variability in signal or band broadening due to excessive Brownian diffusion, which causes this method to be seldom used [6].

A semi-open device means that the paper is open to the air on one side. The other side is usually placed on top a piece of glass or plastic. The glass or plastic that supports the filter paper acts as a heat sink to cool the sample and reduce evaporation. In more complex devices, cooling water can be run under the glass to further prevent evaporation. Semi-open devices can be used in a vertical or horizontal electrophoretic setup and can range from simple to complex. The electrophoresis can be performed over long distances because of the support structure, which allows for better separation of particles with similar mobility with a lower variability in results. The disadvantage of a semi-open setup is the large equipment size needed to perform the separation.

When the filter paper is completely enclosed, it is considered a closed device. The enclosing material can be either a solid material such as glass, or a hydrophobic liquid. If, for example, the paper is sandwiched between two pieces of glass, the edges of the paper are still exposed to the atmosphere, and although this is a small fraction of the surface area, they are a source of evaporation. If the paper is enclosed by a hydrophobic liquid, then the strip is completely immersed in the hydrophobic fluid. The fluid prevents evaporation in two ways: first, it seals the paper from the environment, and second, it acts as a heat sink or a path to a heat sink. Disadvantage of using a hydrophobic liquid include the difficulty of working with materials that can be flammable, such as heptane, which can cause denaturation of proteins, as well as the ability of the hydrophobic liquid to pull molecules from the electrophoretic membrane.

1.4.3 High and Low Voltage Electrophoresis

Most electrophoresis instruments use a low voltage electric field. The difference between a low voltage and a high voltage electrophoresis, is when the field strength

exceeds twenty volts per centimeter. The advantages for high voltage are the fast experiment times compared to low voltage. Usually, high voltage is used with an immersed, closed system which mitigates evaporation and removes excess heat. High voltage systems have been shown to give high resolutions that work better with smaller molecules due to the lower water volumes used in the paper. It is thought that the low amount of water volume causes less transport space between fibers, limiting large particle movement.

1.5 Gel Electrophoresis

Gel electrophoresis has been widely adopted over paper electrophoresis because gel matrices reduce diffusion better then paper matrices [9]. The reduction of diffusion effects is mainly due to a more homogenous matrix, better defined pore size, and more controllable pore sizes. The reduction in diffusive effects allows for better accuracy over paper matrices. The gel matrix has a semi-solid structure with a well-defined average pore size. The pore size allows for different sized molecules to travel faster or slower depending on the size of the molecule relative to the pore size. This type of filtering is called a molecular sieve. The most commonly used gel materials are agarose gel or polyacrylamide gel. Agarose gel is a physically interlocking fibrous structure, where polyacrylamide gel is a cross-linked gel. An example of the structure of gel used in electrophoresis is shown in Figure 1.3.

The type of gel that should be used in gel electrophoresis depends mainly on the size of the particles that are being separated. For smaller molecules, polyacrylamide gel is used because of its smaller pore size. Agarose gel is used for larger molecules. Using

DNA as an example: DNA less than 100 base pairs most commonly use polyacrylamide gel, and long DNA strands that are greater than 100 base pairs most commonly use agarose gel [9].

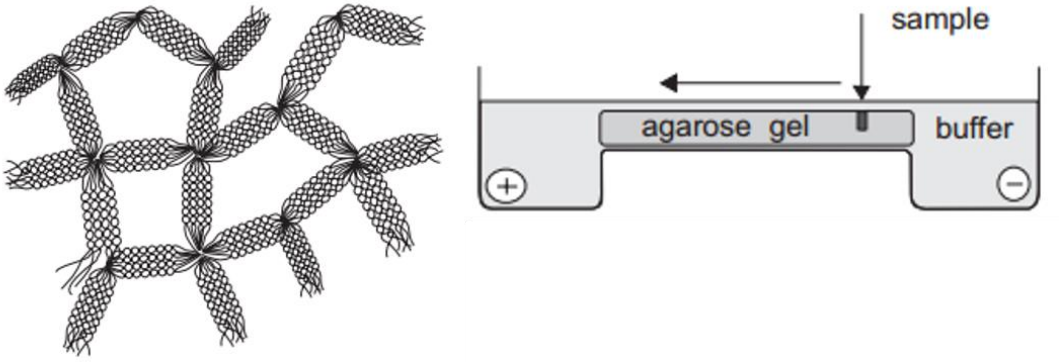

Figure 1.3 Structure and porosity of agarose gel (left) and common horizontal gel electrophoresis test apparatus (right) [9].

1.6 Capillary Electrophoresis

Capillary electrophoresis (CE) is a process that allows for the efficient separation of large and small particles through narrow diameter capillaries between 20 to 200 µm. CE leverages both electro-osmosis flow (EO-flow), which is fluid motion relative to a charged surface induced by an electric field, and electrophoresis [11]. CE can utilize both electrophoresis and EO-flow because, unlike paper and gel electrophoresis, CE is often performed without a sieving medium. The CE process is similar to both gel and paper electrophoresis. An example CE device is seen in Figure 1.4.

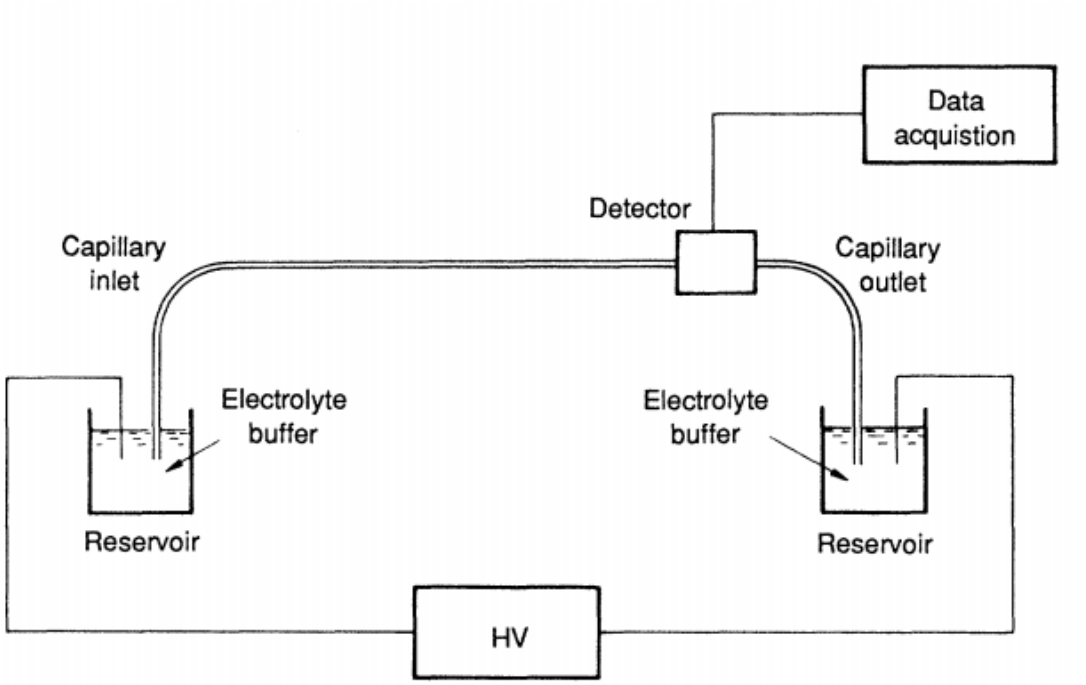

Figure 1.4 General Layout of a CE Device [11].

In a common design, two electrolyte reservoirs are connected by a fused silica capillary. The reservoirs are also connected by electrodes that have an applied voltage. The capillary acts as a bridge that completes the circuit between the two reservoirs. Electrophoretic flow is created when an electric field is applied and the charged particles flow from one reservoir to the other. EO-flow is created from the negatively charged surface of the fused silica capillary which attracts positively charged ions creating an electric double layer. When the electric field is applied, the cations from the double layer flow to the negatively charge electrode, pulling water with them [11]. A UV detector device is usually attached to the capillary for solute detection.

1.7 Microfluidics

Microfluidics is the fluid analog to the IC (internal circuit) chip and involves the manipulation of small volumes of fluid as opposed to electrons. Traditional microfluidic devices (TMDs), devices used in the study of microfluidics, have been in existence for a few decades [12]. TMDs use polymer or glass as a base material [1]. Channels are formed from molds or by using etching techniques to enable fluid routing creating functional diagnostic devices. These devices leverage a number of scientific phenomenon including electric fields, magnetics, pressure, micromechanical valves, micro-pumps to filter, and flow sensors to manipulate fluids, solutes, and analyze samples [13].

TMDs carry a wide variety of functions including electrophoresis, polymerase chain reaction (PCR), immunoassays, protein separation, and cell manipulation and analysis [14]. These functions make TMDs very useful, in particular for portable systems and in developing countries where access to equipment for these tests is limited. However, TMDs can rarely be re-used owing to biological materials adhering to channel walls and cross-contamination issues. While some TMDs have been shown to yield accurate results, they require specialized equipment, precise machining, and specialized training to manufacture. These issues has given rise to the need for the development of simple, rapid, low cost paper assays, such as, microfluidic devices or microPADs.

In microPADs, the base materials are cellulose and nitrocellulose membranes, and the geometric features, e.g. channels, are printed or applied to the surface using a hydrophobic material. Depending on the process, further treating such as baking or exposure to solvents may be needed to create microfluidic structures. Processes used to create a hydrophobic barrier include photolithograph, plasma etching, wax printing, and

more [1]. In TMDs, fluid is usually driven by an applied pressure, whereas in microPADs, fluid is driven by capillary action.

1.8 Immunoassay

Immunoassays are tests that utilize biochemical processes to detect target molecules with immunoglobulins. LFA devices generally follow the same format but can vary in design. The first part of the device is called the sample pad, which is where a sample is introduced into the device. The sample flows down the membrane until it reaches the conjugate pad. The purpose of the conjugate pad is to release detector reagents into the sample as it flows through [15]. The detector reagents then bind to specific target molecules or cells within the sample. After flowing through the conjugate pad, the sample flows onto a membrane until it reaches the detection region of the device. The detection region consists of at least two lines, a test line and a control line. The test lines determine if the sample is present, and the control lines determine if adequate flow is achieved for correct detection in the test region [16]. The final part of a LFA device is the absorbent pad whose purpose is to provide extra volume so that capillary flow can continue by drawing more of the sample across the detection line. LFA devices can be broken down into two main types: lateral flow immunoassays (LFI) and nucleic acid lateral flow immunoassay (NALFI).

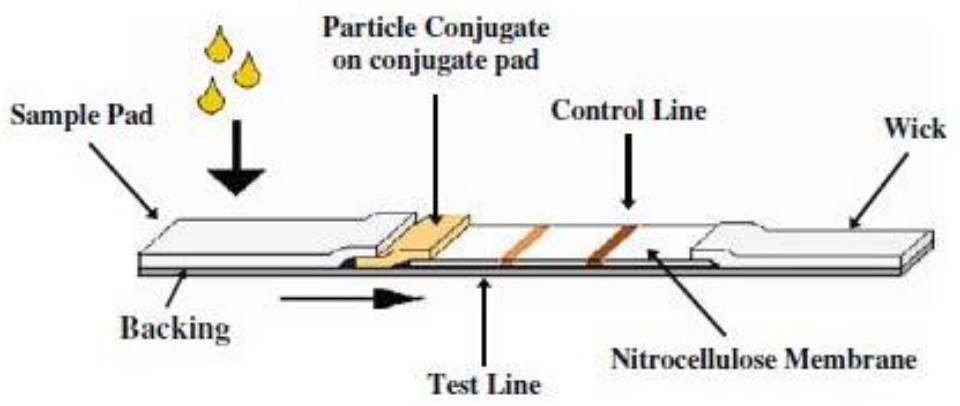

Figure 1.5 General lateral flow assay design including sample pad, conjugate pad, membrane, absorbent pad(wick) and backing [17].

1.8.1 Lateral Flow Immunoassay

LFIs are used to determine if a sample contains or lacks a target compound. A compound is targeted depending on its availability to bind to particular antibodies. If a compound has two sites for independent antibody binding, then a sandwich LFI can be made [16]. In this method, one antibody is applied to the test region of the membrane and the other antibody is in the conjugate pad. The antibody on the conjugate pad is usually tagged with a color or fluorescent nanoparticle for detection of binding. If a target compound is present, as the sample flows over the conjugate pad, the colored nanoparticle antibody will bind to the compound. When the target compound reaches the detection region, it will bind to the antibodies and create what is called a detection line [17]. The compound is now fixated in the test region and the color from the nanoparticle is visible. If the compound is not present, binding will not occur and there will be no color change at the detection line.

Another type of LFI test is based on competitive binding of an immobilized antibody in the detection zone. The target compound and a colored nanoparticle both have the same binding for the antibody and compete for binding. Antibodies are in the detection zone, while the colored nanoparticle is within the conjugate pad. As the sample flows over the conjugate pad, the sample mixes with the labeled nanoparticle and flows to the detection region. When the sample reaches the detection line, the immobilized antibodies will either bind to the target compound or the labeled nanoparticle from the conjugate pad. If the sample is positive for a compound, then the target and the labeled nanoparticle will compete for binding sites of the immobilized antibody in the test line [17]. As the sample reaches the control line, the labeled nanoparticles will bind with a second type of immobilized antibodies that are specific to only the nanoparticles. The control line indicates that enough functioning nanoparticles were used for a valid test. In this test, it is better to have higher concentrations of the sample than the nanoparticles to allow for accurate interpretation of results. A positive result using competitive binding is read as a lack of signal on the test region. Figure 1.6 shows an example of competitive and sandwich LFIs.

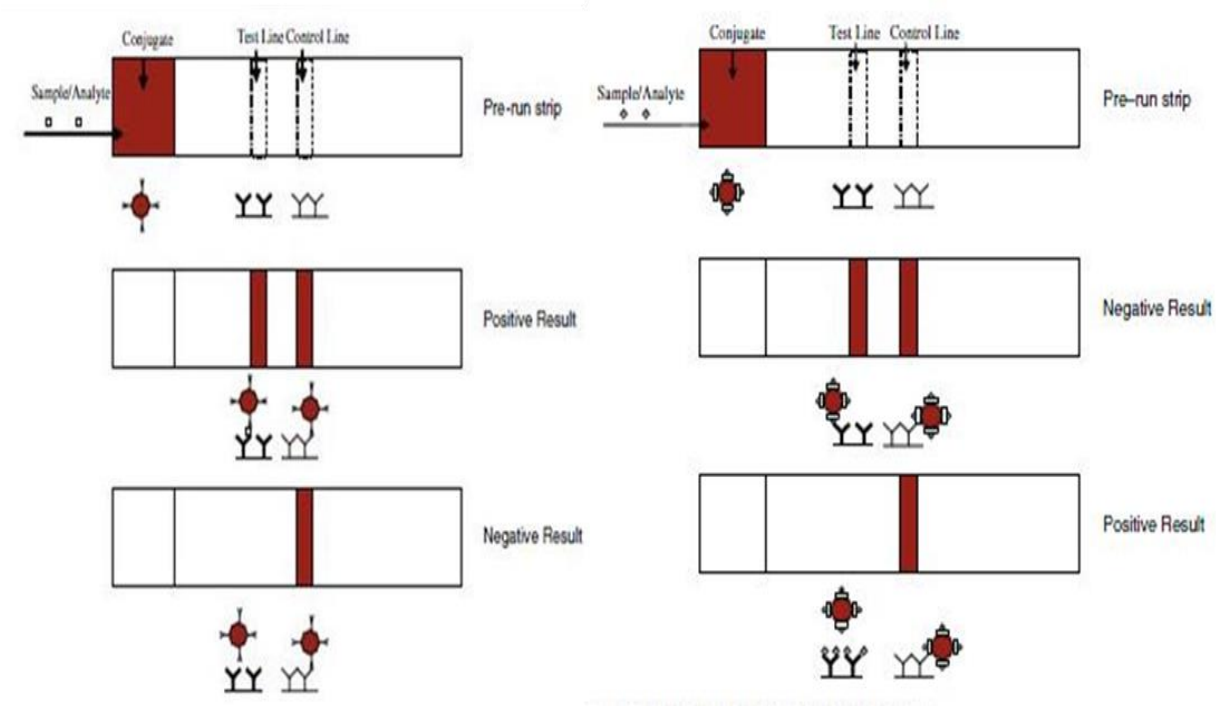

Figure 1.6 The sandwich anti-compound assay (left) and the competitive assay (right) showing results for positive and negative samples [17].

1.8.2 Nucleic Acid Lateral Flow Immunoassay

NALFIs differ from LFIs by what the test is looking for and how results are detected. In NALFIs, the target is a pathogen, compared to a compound in LFIs. To target a pathogen, specific amplified, double-stranded nucleic acid sequences are used [18]. This process has a different set-up, but most use single stranded oligonucleotides attached to a silver, gold, or fluorescent particle that bind to target DNA and another oligonucleotides attached to the membrane [14, 16]. Similar to LFIs, a positive reading is indicated by the presence of nanoparticles in the detection line. Lastly, the control line in NALFIs bind the oligonucleotides to indicate a successful test.

1.9 Materials

MicroPADs are composed of different parts that perform different functions within a device. This means that different materials can be used in different parts of the device. This variability in material selection allows for adjustment of device properties depending on the type of test. There are a number of materials available for each part of microPADs. The next section will discuss the various materials for the different sections of microPADs and why they are used.

1.9.1 Paper Membrane

The membrane material is the most important part of a microPAD. It occupies the majority of space of the device and has the largest effect on sample flow. The most common materials used for the membrane are cellulose and nitrocellulose [16]. Other less common materials include nylon, polyethersulfone, and polyetherlyne [15, 16, 19, 20]. Nitrocellulose has many properties that are beneficial for microPADs. First, it is a porous material. The pores in the membrane affect capillary flow, and by using nitrocellulose with different pore sizes, the flow in the device can be controlled [15]. The flow time of a sample controls how long the sample is in contact with reagents from the conjugate pad and detection region. It is important for flow times to permit ample time for reagents to bind to target compounds. The pores also affect the size of particles that can efficiently make it through the membrane. For example, if a pore size is too small for a particular sample, the pores may get clogged and prevent target compounds from reaching the detection region [17]. Second, nitrocellulose has active sites within it that allow for easy immobilization of reagent for detection lines. Third, the mechanical properties of nitrocellulose provide a matrix of adequate strength that limits tearing of

microPADs during printing of the device. Additional strength can be added to the materials with the addition of a backing of a stronger material, usually a polymer. Membranes can be purchased already with a plastic backing, or they can be manually backed with tape. Finally, if a baking process is used, the ignition point of the membrane needs to be taken into account. The ignition temperature of nitrocellulose is about 200^{o} Celsius; however, baking has been shown to be successful with temperatures as low as 125^{o} Celsius [3]. This allows impregnation of wax barriers with limited risk of burning the material.

1.9.2 Conjugate Pad

The conjugate pad provides a medium for which reagents can be introduced into a sample as the sample flows through it. The focus of material selection for the conjugate pad includes ease of reagent addition into the pad as well as how the material releases the reagents as a samples flows through it. The material chosen is usually a fibrous matrix with common types including cellulose, fiber glass, and polymers such as polyester [15]. Another desirable property of the material chosen for conjugate pads is the lack of the ability to bind to proteins or reagents as they enter the pad so that potential targets are not lost before detection. Holds-up volumes, or the amounts of fluid that can be stored in the membrane, are also important because it will determine how much reagent can be added to the pad. Additionally, since the conjugate pads are cut into small pieces, tensile strengths are an important factor to consider as weaker materials may fall apart and be difficult to cut. Some materials may use adhesives to keep the fibers held together; however, it is important that the adhesive is not released into the sample. Table 1.1 compares properties of three common conjugate pad materials.

Table 1.1 Properties of Suitable Conjugate Pad Materials [15].

Non-woven Material	Brief Description	Key Benefits	Key Liabilities
Glass fibers	100 – 500 µm thick, may contain binders to hold fibers together	Good hold-up volumes, low nonspecific binding	Poor tensile properties, difficult to slit and web handle
Cellulose filters	300 – 1000 µm thick, compact fibers of consistent density	Very low nonspecific binding, normally very uniform	High hold-up volumes (>50 µL/cm²), can be very weak when wet
Surface-modified polyester	100 – 300 µm thick, hydrophilic polyester filters	Low nonspecific binding, excellent tensile strength and web handling	Low, and somewhat variable, hold-up volumes (<15 µL/cm²)

1.9.3 Sample Pad

The main purpose of the sample pad is to receive the sample, incorporate it into the device, and distribute it into the conjugate pad [15]. Sample pads do not necessarily need to be different from the membrane material, depending on the application. Most importantly, the sample pad needs to easily absorb a sample and its constituents. For instance, whole blood has a large portion of solutes, mostly red blood cells, which can clog the membrane. In this case, the sample pad must be designed to filter the cells out but allow the blood plasma to continue through to the conjugate pad [15].

1.9.4 Absorbent Pad

The purpose of the absorbent pad is to promote capillary flow and sample movement down the device. Without an absorbent pad, the flow would stop before a large portion of the sample passed the detection region [15]. Absorbent pads act as extra volume to continue the capillary flow and as a buffer for sample size, making a range of sample sizes usable. Absorbent pads are important to include in the design of the device and follow the same general material selection guidelines as the sample pad except that they will not be treated with reagents.

1.10 Paper Microfluidic Printing Techniques

As described above, there are a number of methods available to create paper microfluidic devices. Depending on the needs and requirements of the device, environmental factors, and available equipment, different manufacturing techniques may be advantageous. Most manufacturing techniques involve setting down a hydrophobic barrier and impregnating the barrier material into the membrane pores. The different manufacturing approaches are better for various properties such as minimum channel widths for fluid flow and minimum hydrophobic barrier widths to keep fluid from escaping past the barrier. Other methods may require the need for solvents and polymer contact [1]. There are many techniques including cutting, plotting, photolithography, plasma treatment, inkjet etching, and wax printing each with their advantages and disadvantages. Only wax printing will be discussed as it was the method used in this thesis.

1.10.1 Wax Printing

Wax printing can be performed using commercially available printers. A printer that can be used is the Fuji Xerox Phaser printer, which can print a wax based ink onto a paper. However, the wax does not fully penetrate the paper since the printer prints the wax on top of the paper. To get complete impregnation of the wax, after printing, the paper needs to be baked up to a few minutes [3]. At this point, the chip is finished. With only two steps, the process is very simple compared to the other techniques. It also does not require any solvents. Even more, the printer can be used straight out of the box. Since multiple devices can be printed per page, large quantities can be produced. The shelf life of the paper-based lateral flow assays can range between 12- 24 months without

refrigeration, allowing large quantities to be stored ahead of time and used as needed [17]. The process is rapid, can be performed almost anywhere, requires little training, and is cheap. Disadvantages of wax printing include inability to produce sensitive quantitative results. Another issue with wax printing is spreading of the wax when baking the paper. This causes smaller channels and geometries than what is originally intended. However, the simplicity of use and the ability to make complex channels make wax printing a strong candidate for microPADS manufacturing in developing countries.

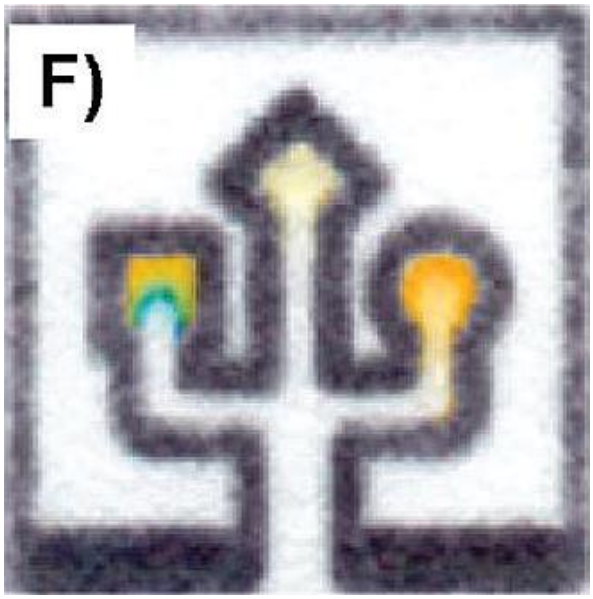

Figure 1.7 Paper microfluidic device fabricated using wax printing method [1].

1.11 Electric Fields in Microfluidics

Traditional microfluidic devices utilize electrical fields to perform tasks such as diverting fluid flow or detecting targets in a sample. TMD platforms make it easy to incorporate an electric field into the chip. MicroPAD platforms, however, are more difficult to incorporate an electrical field because of various design reasons. One problem is joule heating that happens as the electric fields passes through the sample

causing the sample to heat up [21]. The heating will cause the sample to evaporate, possibly, before it reaches the test line. TMDs do not experience this problem as intensely because the sample is completely enclosed in the device, preventing evaporation. In microPADs, wires and circuitry cannot be incorporated into the device as easily as in TMDs. Problems arise from the hydrophobic barrier because it is also an electrical insulator. Completing the electrical circuit means the barrier will have to be bypassed in order for the electric field to reach the sample. One way this has been done is by using Ag/AgCl ink to make electrodes and placing them over the top of the fluid channels [22]. Electrodes have also been made by screen printing a layer of lead mixed with carbon ink and a second layer of Ag/AgCl over the channels [23].

1.11.1 Electrochemical Sensing

The usage of electrical fields in microPADs has been mostly limited to electrochemical sensing. Electrochemical sensing is a technique used to detect a target compound by means of electrical and chemical reactions. This method usually uses three electrodes: a working electrode, a counter electrode, and a reference electrode [23]. When a voltage is applied to the electrode, the compound of interest interacts with an enzyme, causing a change of amperage that can be measured. Change in amperage corresponds to the amount of compound present; the higher the concentration of the target molecule, the larger the resultant current response. This technique has been shown to be successful at detecting the amount of sugars in a sample, for example glucose and lactate. An example of an electrochemical sensing device is shown in Figure 1.8 [23]. This kind of sensing can give precise quantitative values for the amount of compound present.

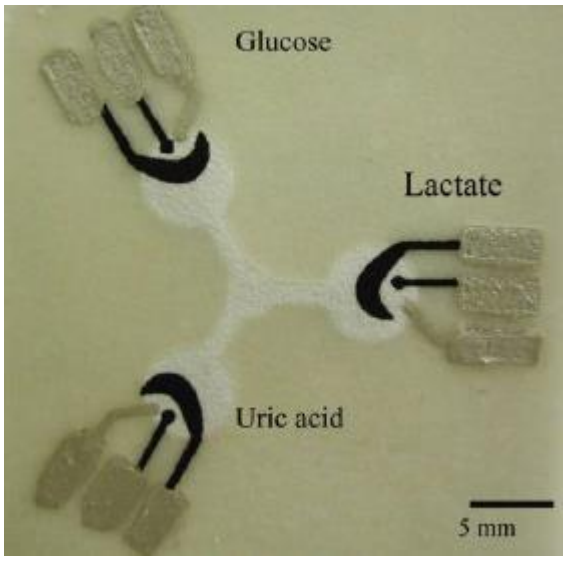

Figure 1.8 Example of electrochemical sensing microPAD [23].

1.11.2 Electrophoresis in TMDs and microPADs

One electrical technique that is commonly used in TMDs, and has only recently been incorporated into microPADs, is electrophoretic flow or electrophoresis[2]. This is the use of electrical forces to control the flow of charged solutes in a fluid. The application of electric fields applied to TMDs is well established as a separation technique [24]. The fields can act as separate pumping forces and have the ability to be miniaturized. Electrophoretic separations have been used for immunoassays and pre- and post- treatments of samples in TMDs. Issues with electrophoretic flow include many of the same problems as in electrochemical sensing, such as joule heating and bypassing of a hydrophobic barrier. A difference between fluid flows in TMDs versus microPADs is that in TMDs, flow can be controlled by pressure gradients that can be actively changed. In microPADs however, the fluid flow is controlled by capillary action and cannot be actively changed. For this reason, incorporation of the electrophoretic fluid flow in microPADs will probably be more limited than TMDs. Although Electrophoresis has

been applied to microPADs, theory for predicting electrophoretic separations have not been defined in microPADs. Therefore, it would be beneficial to create a theory for electrophoretic separations in a microPAD.

1.12 Thesis Outline

The following chapters of this thesis will attempt to verify and answer the driving questions of this thesis. Chapter 2 discusses the theory used to predict drift velocities and electrophoretic separation velocities. Chapter 3 will discuss the selection of materials used in manufacturing of microPADs and measure properties of the materials that will be needed in following sections for theoretical predictions. Chapter 4 covers the microPAD design and fabrication protocol. Chapter 5 contains velocity measurements on paper membrane and compares them to theory. Chapter 6 uses the results of Chapter 5 to predict the transverse electrophoretic separations and verify results. Finally, Chapter 7 contains the conclusions, discussion on limitations, and future work.

CHAPTER 2: **THEORY**

2.1 Theory

Fluid transportation through a microPAD has a number of mechanisms that drive the process. These mechanisms are effected by many external and internal factors. External factors that can influence flow include things such as temperature, membrane material and structure, pH, humidity, electric field strength, and ionic concentration [6, 17]. Internal factors are factors that pertain to the molecule being studied. Internal factors include size, electrical charge, shape, and tendency to dissociate or denature [6]. Taking into consideration all the factors would be difficult and outside the scope of this thesis, so the theory for this thesis is presented in the next few sections and will only look at the factors with the greatest influence on particle transportation and fluid flow.

2.1.1 Capillary Flow

The porous structure of a cellulose membrane causes a network of tubes or channels that the fluid and the particles carried by the fluid can flow through. The interaction of the fluid particles on the wall of the tubes causes capillary action, which drives fluid flow in a porous matrix [25]. Capillary action is most commonly known in a vertical application where it drives fluid upward until the weight of the fluid balances the capillary force. In a horizontal position, gravity is no longer a hindering factor, allowing capillary action to act more as a fluid pump moving fluid continuously through the capillary and only stopping when the capillary becomes saturated with a liquid.

Flow through a capillary can be simplified to be modeled as flow through a cylinder. Flow in a single cylinder, Q, can be defined by Eq. (1) [25] where R is the

radius of the cylinder, ΔP is the change of pressure across the length of the tube, μ is the viscosity of the solution in the cylinder, and L is the length of the tube.

$$Q = \frac{\pi R^4 \Delta P}{8\mu L} \qquad (1)$$

Eq. (1) is then divided by the cross sectional area of the cylinder,πR^2, and the pressure drop,ΔP, is substituted with the Young -Laplace pressure drop shown in Eq. (2).

$$\Delta P = \frac{2\gamma \cos(\theta)}{R} \qquad (2)$$

The Young –Laplace equation uses surface tension γ and the contact angle θ to calculate the pressure change. The resultant of combining Eq. (1) and (2) solves for the velocity in a cylinder caused by capillary flow. If the path of the cylinder is not a straight line, the movement through the capillary is hindered. To represent the reduced flow, a variable is added called tortuosity τ, which reduces flow based on how difficult the capillary is to flow through [25]. The resultant equation shown in Eq. (3) represents the velocity through a single capillary.

$$\frac{dL}{dt} = \frac{R^2 \gamma \cos(\theta)}{4\mu L \tau} \qquad (3)$$

Cellulose, however, is composed of many small capillaries that form a complex network of channels for fluid transport. Since Eq. (3) is only valid for a single channel, its usefulness in predicting bulk velocity in a membrane with a large number of capillaries with nonlinear paths is limited.

2.1.2 Electrophoresis

The flow of charged particles in a porous medium will be acted on by many forces. The hydrodynamic resistance will resist the motion of particles caused by

electrophoresis, and the forces will balance, resulting in a terminal velocity and is described by the electric mobility equation seen in Eq. (4) [25].

$$u_E = \frac{qE_x}{\xi} \qquad (4)$$

The net velocity u_E is caused by the electric field strength E_x acting on the charged particles q and resisted by the hydrodynamic resistance ξ. The movement of particles caused by the interaction of an electrical gradient is called electrophoresis. The hydrodynamic resistance is given by Stoke's drag holds true for laminar flow and in pure solution shown below in Eq. (5) [25] where a is the radius of the solute, which in this thesis will always be an Orange G dye particle, and μ is the viscosity of the fluid, in this case, water.

$$\xi = 6\pi a\mu \qquad (5)$$

By substituting Eq. (5) into Eq. (4), the equation for describing the velocity of charged particles in a fluid is found [25]. To use the equation in a fibrous medium, it needs to be modified to account for the interactions of the particles inside the membrane and the fibrous structure of the membrane [25]. This modification to stokes drag is done by adding what is known as the Brinkman correction. The Brinkman correction is added to the hydrodynamic resistance equation, which takes into account the effects of the membrane fiber interaction with the solutes and is shown below in Eq. (6) [26].

$$\xi = 6\pi a\mu \left(1+\propto a + \frac{(\propto a)^2}{3}\right) \qquad (6)$$

The brinkman correction uses the Brinkman Screening Length $\propto$ and the solute radius a to increase the hydrodynamic resistance. By substituting the hydrodynamic resistance containing the Brinkman correction back into Eq. (4), the velocity of the particles caused by the electric field in a fibrous medium is attained and is shown in Eq. (7).

$$u_E = \frac{qE_x}{6\pi a\mu\,(1+\propto a+\frac{(\propto a)^2}{3})} \qquad (7)$$

2.1.3 Microfluidic Chip Theory

The first step for understanding the separations of particles on a microPAD using electrophoresis was to create a theory that could predict the electric field strengths required for the separation of those particles in the electrophoretic zone of the microPAD. The theory would have to take into account the horizontal and longitudinal portions of the electrophoretic zone. The horizontal component consists of the application of the electric field, which takes into consideration the electrophoretic drift velocity defined by Eq. (7) and the horizontal distance of the electrophoretic zone. The vertical component is the amount of time the fluid takes to travel the length of the electrophoretic zone, or residence time, which is transverse to the electric field gradient. Measurement locations are depicted in Figure 2.1.

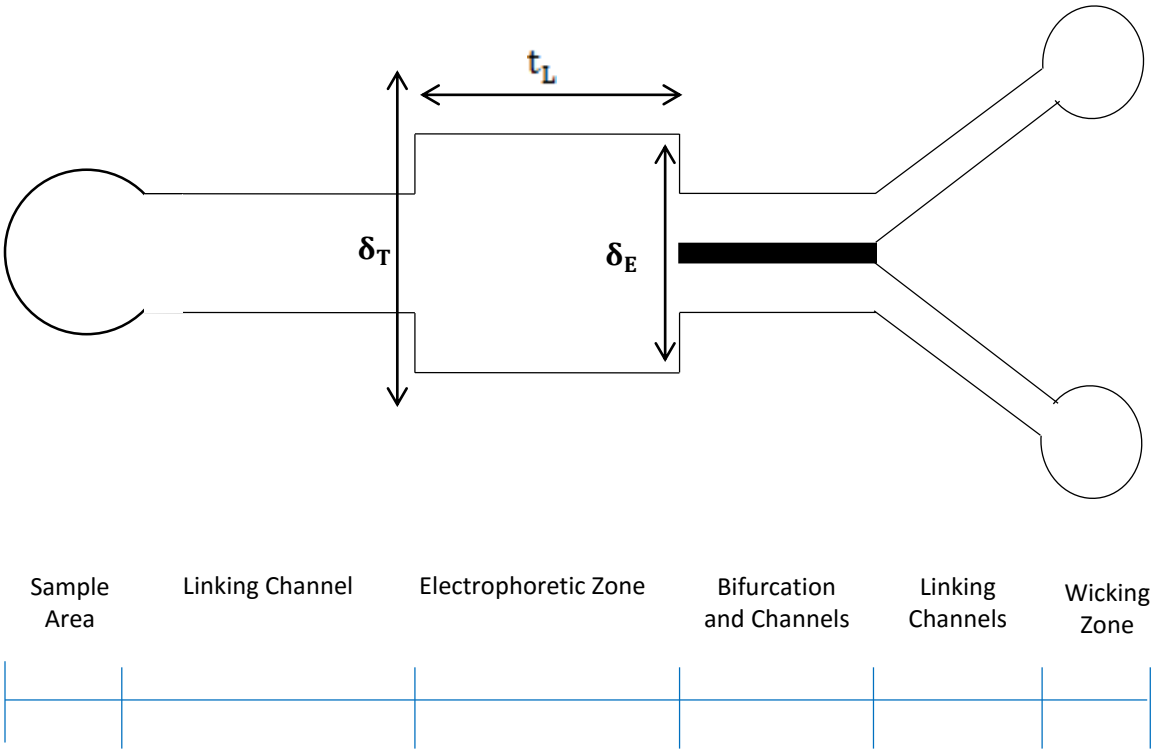

Figure 2.1 Image shows the where the variables δ_E , δ_T, and t_L are measured from.

The theory needs to predict the necessary voltage that should be applied to the electrophoretic zone based on the calculated separation, or drift velocities. By rearranging Eq. (7), the electric field magnitude can be solved for by replacing the electric field strength, E_x, with the applied voltage divided by the distance between the electrodes, $\frac{Vap}{\delta_E}$. Solving for the applied voltage, V_{ap}, results in Eq. (8).

$$Vap = \frac{u_E \delta_E 6\pi a\mu \left(1+\propto a+\frac{(\propto a)^2}{3}\right)}{q} \qquad (8)$$

u_E is the electrophoretic drift velocity caused by the electric field calculated in Chapter 4. The minimum allowable drift velocity to successfully divert the dye into a single channel can be determined by dividing the distance the charged particles have to travel transverse to flow, δ_T, by the residence time it takes for the fluid to pass electrophoretic zone longitudinally, t_L. This calculation is seen in Eq. (9).

$$u_E = \frac{\delta_T}{t_L} \qquad (9)$$

By substituting Eq. (9) into Eq. (8) and solving for V_{ap}, an equation for predicting the necessary applied voltage can be formed. This is shown with Eq. (10).

$$Vap = \frac{\delta_T \delta_E 6\pi a\mu \left(1+\propto a+\frac{(\propto a)^2}{3}\right)}{q} \qquad (10)$$

The steady state and the initial condition change the amount of voltage required to successfully separate the dye. In the initial condition, the transverse distance, δ_T, is large because it is the entire length of the channel. Once the chip reaches steady state, the distance, $\boldsymbol{\delta_T}$, decreases the length from the electrophoretic channel wall to the far inlet channel wall. The decrease in length means that that the velocity used to capture the dye will be greater than the velocity needed to separate the dye at steady state and will be proportional to $\delta_{T-S.S.}$ divided by $\delta_{T-initial}$.

CHAPTER 3: **MATERIAL SELECTION**

The first part of this thesis was to develop a protocol for creating a microPAD that could support electrophoresis. Before a fabrication protocol could be made, materials needed to be selected, and their properties measured and checked for compatibility with each other. Once the materials were chosen, a fabrication protocol was created.

There are many different methods for creating paper based chips; however, techniques that use wax printers have been shown to be the quickest, easiest, and least expensive [27]. For this reason, wax printing is an ideal method for the fabrication of microPADs. In this thesis, a protocol for printing and baking paper chips with a wax printer was created based on methods from the studies of Y. Lu *et al*. Next, the protocol was expanded to introduce an electric gradient to the chip. A protocol for applying the electrodes was added to the fabrication protocol. After the fabrication protocol was completed, a chip design was created to allow for the separation of O.G. dye by electrophoresis. Finally, flow times through the channel were measured to be used in theoretical predictions used in future chapters. This section of the thesis will discuss in detail the steps taken to select materials and fabricate a microPAD with electrophoresis.

3.1 Material Selection

Each section of the microPAD has a different function and thus different material properties are required. This section discusses the properties of suitable materials and how those properties will be measured and compared.

3.1.1 Membrane Materials

Membrane materials require different properties for best sample flow and compound detection to occur. For the sample pad, reagent immobilization needs to be low; however, in the detection region it needs to be high because the immobilization of the reagents allows for detection of targets in the test line [17]. Electrophoresis in microPADs is most likely to be used as a pre-detection treatment to increase target concentration or remove unwanted particles. The electric field, in this case, would then be applied on the sample pad, and the most common materials are cellulose and woven meshes. Cellulose chromatography paper is a far superior choice as it is less expensive than woven meshes and is much more suitable for printing.

Whatman Company sells a wide range of papers for lateral flow assays with varying properties. The membranes chosen to be investigated were Whatman 3001-861 Grade 1 and Grade 3 Cellulose Chromatography Paper. Both of these papers are widely used in analytical techniques and have average properties, for instance, a medium flow retention and flow rate. Another important property to consider is paper thickness. Paper that is too thick will jam in the printer and require a large amount of sample to flow through the paper. However, if the paper is too thin, the paper will have poor strength properties and may tear in the printer and require low amounts of sample that may produce inaccurate results.

Whatman Chromatography papers have a range of thicknesses and flow rates. 20 cm by 20 cm sheets of Grade 1 and 3 were used for testing. Grade 2 was not used since the properties are almost identical to Grade 1. Grade 4 was not tested because it was thought that its high flow rate properties could cause problems for velocity

measurements and applied voltages in later sections. The thickness of the paper for Grade 1 was the thinnest offered at 180 µm. Grade 3 had a larger thickness of 360 µm. Test printing with Grade 3 paper almost always resulted in a paper jam. Grade 1 only occasionally caused paper jams, making it a better choice than Grade 3 paper. A comparison of flow rates and thicknesses is shown in Table 3.1.

Table 3.1 Comparison of Whatman cellulose chromatography filter paper grades 1-5.

Grade	Thickness(µm)	Flow (mm/min)
1	180	130/30
2	180	115/30
3	360	130/30
4	210	180/30

3.1.2 Fiber Measurement with Scanning Electron Microscopy

Images taken with scanning electron microscopy (SEM) can show the micro- and nano- structure of a material [28]. SEM enhances a materials structure with a magnification of about 10 to 20,000 times [28]. The detailed resolution of SEM allows for analysis of a material or specimen surface structure revealing information on porosity, fiber diameter, and composition. SEM imaging of the cellulose allowed for visualization of the overall microstructure and was used to take fiber diameter measurements. The diameter was used in predicting the hydrodynamic hindrance in particle flow caused by the fibers.

In order for a sample to be imaged, the sample needed to be placed in a vacuum where a beam of electrons focused by electromagnets shot at the sample. The focusing of the electromagnets controlled the diameter of the beam, which defined the resolution of

the sample. The electrons then either bounced or were absorbed or emitted by the sample. The electrons that bounced off or were emitted by the sample are called “back scattered electrons” and were detected by the SEM. The detectors measured the location of emission, energy, and density of the electrons and used the information to assemble a detailed image of the sample [28]. A SEM sample cannot be wet because the vacuum and heating caused by the electron beam will cause the water to evaporate from the sample. The water being released by the sample can ruin the sample or the sensitive equipment.

Once an image was rendered by the electron microscope, the fibers could be measured using the image analysis program [Image J]. The magnification used on the SEM was 500x. In Image J, the measuring tool first had to be normalized using the SEM scale bar on the image. Next the image was broken into quadrants and zoomed in to make more accurate measurements of the individual fiber diameters. The fiber measurements were taken perpendicular to fiber length, and some fibers were measured multiple times in different areas. A total of 40 measurements, 10 measurements from each quadrant, were taken and averaged together to determine the mean fiber diameter. From the measurements, the average fiber diameter was calculated to be 14.6±0.1 micrometers and had a standard deviation of 4.76 micrometer. The average diameter is used to calculate theoretical separation velocities in future sections.

Additionally, the fiber radii of the cellulose paper were inspected visually to check for any net fiber alignment and overall structure. It could be seen that fiber radii varied not only among different fibers, but also along individual fiber strands. Cellulose

can also bifurcate causing two smaller radius fibers to form from one. An example of a SEM image of fibers can be seen in Figure 3.1. From inspection it is clear that the fibers did not have a net alignment or orientation that could affect fluid flow.

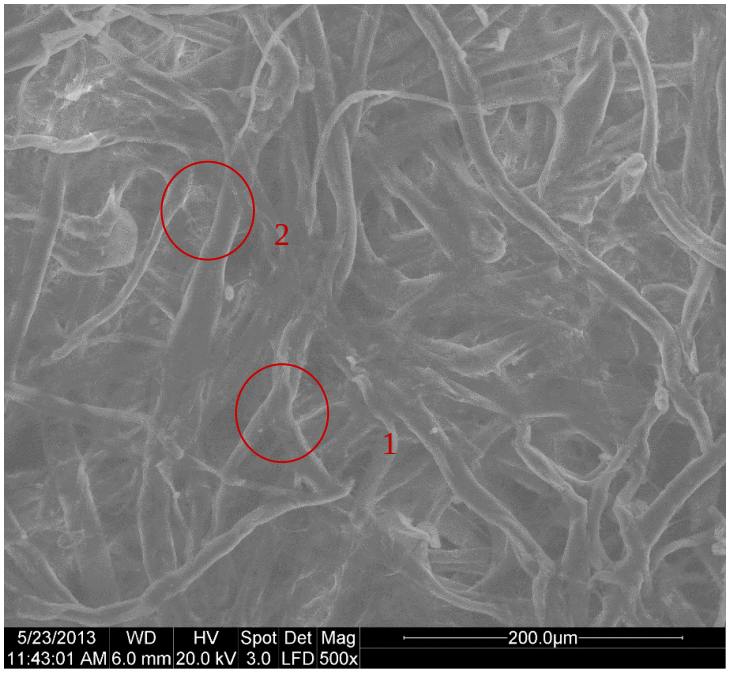

Figure 3.1 SEM image of Cellulose membrane (1) bifurcation of Cellulose fiber (2) thinning of fiber diameter.

3.1.3 Conductive Materials

Finding a way to conduct electricity around the wax layer was one of the major hurdles in this thesis. It was found that the wax could be bypassed by laying a conductive material over the wax so that it contacted the fluid of the channel. Three materials where looked at to bypass the wax: copper wire, silver conductive epoxy, and colloidal graphite paste. Copper wire was bent into an 'L' shape and placed into the electrophoretic zone of the chip, and the wire was held down with tape. The silver conductive epoxy, or cold solder, is a two part mixture that solidifies over 5 hours and has very good conductive

properties. To apply the solder, the two parts were mixed together in a dish and then applied over the edges of the electrophoretic zone so that the cold solder barely contacted the paper membrane. The colloidal graphite paste uses conductive graphite to transmit the voltage across the electrophoretic zone. The paste was applied in a similar fashion as the cold solder.

To find the best material for a microPAD, five trials were run with each type of material. The materials were scored based on several categories. The first category was if the material could conduct electricity across a channel. Second, the material was checked to see if the electrode material still allowed flow through the channel. The third and fourth categories were how easy it was for the material to be applied to the paper membrane and the cost of the material. The materials were rated in these categories, and the best material was chosen.

Table 3.2 Criteria for selection of electrode material.

Criteria				
Material	Conductive	Allows Fluid flow	Ease of Application	Cost
Copper Wire	+	+	-	+
Cold Solder	+	-	-	-
Graphite	+	+	+	+

Conductivity was measured using resistance values: the lower the resistance, the higher the conductivity. All materials compared were conductive. Copper had the lowest resistance of about 0.00005 ohms/cm. Next was the cold solder with a resistance of 0.017 ohms/cm. Last was the graphite paste with a resistance of 24000 ohms/cm. Although graphite had a very high resistance, it is still conductive. In regards to fluid

flow, both the copper wire and the graphite paste allowed fluid to flow through the channels without signs of blocking. The cold solder, however, completely blocked the channel. An example of the cold solder blocking the channel can be seen by the discoloration of the paper in Figure 3.2.

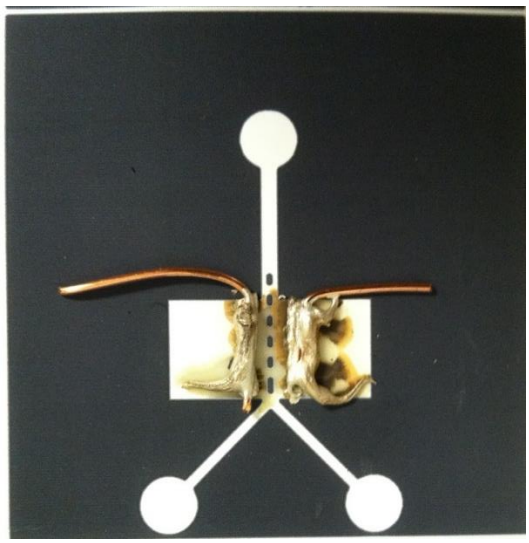

Figure 3.2 A test application of cold solder electrode on a paper chip after 24 hours. The dark areas around the cold solder show leaching of paste into the chip, ultimately blocking the inner channel and possibly contaminating the chip.

As far as application of the material, the application of the copper wire and the cold solder to the membrane proved to be quite difficult. Since the copper wire did not have an easy way to be attached to the membrane, tape was used to help secure it, however the wire would easily dislodge from the paper with minimal effort. Additionally, it was difficult to make the wire lie flat across the entire length of the channel, disrupting the even distribution of the electric field across the channel.

The cold solder was difficult to apply because, first, there was not an easy way to apply it evenly to the membrane, and second, the cold solder took over 24 hours to completely dry, significantly increasing fabrication time. The graphite paste, unlike the other materials, was very easy to apply to the membrane and dried within minutes.

The Pelco Colloidal Graphite came with a brush and an extender solution, which allowed for a change in the viscosity of the paste. Using the brush, it was possible to apply thin, even layers across the channel. Lastly, the cost of the materials was taken into consideration. Copper wire and graphite are significantly less expensive than cold solder. The cost for copper was 4.36 grams per dollar; for graphite the cost was 0.33 grams per dollar; and for cold solder the cost was 4.14 grams per dollar. All these results lead to the graphite paste being used for the electrode material.

3.1.4 Dye Selection

The next material selection was choosing a dye. A dye was necessary in order to visually measure the separation velocity of a fluid. One criteria for selecting a dye was for the dye to be small enough in size that it did not get clogged in the fibers of the channels. Second, the dye needed to be easily visible or colormetric so that velocity measurements could be taken. Third, the dye needed to have a charge so that it would be attracted to an electrode and separate. There are many dyes on the market that are designed specifically for electrophoresis and are also colormetric. Dye Orange G was chosen out of other suitable dyes because it was the smallest size. An important property of the dye necessary for theoretical calculations is the radius and it was estimated using Eq. (11) shown below where a is the particle radious, MW is the molecular weight of the particle, and ρ is the density of the particle.

$$a = \left(\frac{3MW}{4\pi\rho N_A}\right)^{\frac{1}{3}} \qquad (11)$$

The dye comes in a powder form and needs to be mixed with water to create a useable dye solution. O.G. dye was made in 50 ml batches of either 10 mM by mixing 0.226 g of dye or 1 mM by mixing with 0.0226 g of dye with 50 ml of DI water. The protocol used to create the dyes can be found in Appendix A.1.

Orange G has a relatively small molecular weight of 452.37 Daltons with a molecular formula of $C_{16}H_{10}N_2NA_2O_7S_2$ [29]. Using Eq. (11) and the molecular weight, the radius of the dye was approximated to be 0.564 nm for pure O.G. The structure of O.G., shown in Figure 3.3, consists of three benzene rings that contain six carbon atoms and six hydrogen atoms. Two of the benzene rings are connected by sharing two of the carbon atoms, and the third is connected to one of the benzene rings by two nitrogen atoms. The benzene ring not bound to nitrogen has two sulfur atoms bound to it. Each sulfur atom is double bound to two oxygen atoms and a single is bound to oxygen, which has a sodium atom attached to it.

When Orange G is placed into water, the two sodium ions disassociate from the oxygen, giving the dye a net negative 2 charge or -3.204 E-19 coulombs. The disassociation also effects the MW of O.G. causing it to lose 46 Daltons. The MW of the O.G. in water becomes 406.38 Daltons, and the radius is estimated to be about 0.49 nm. The conductive properties are the most important aspect of the dye for this project since the charge allows the dye to be separated in an electric field. The color of the dye is a brilliant orange but can change with pH. At a pH higher than 9, the dye becomes red. At

1 mM or 10 mM, the pH of the dye is about 7 and the dye color was clearly orange and easy to see with the naked eye.

The ability of the dye to enter the paper matrix is also an important quality of dye. This is why the radius of the dye was considered in the selection process so that the dye did not clog the pores of the paper. The dye was shown to easily enter the paper membrane and did not show any signs of clogging while the electrode materials were being tested.

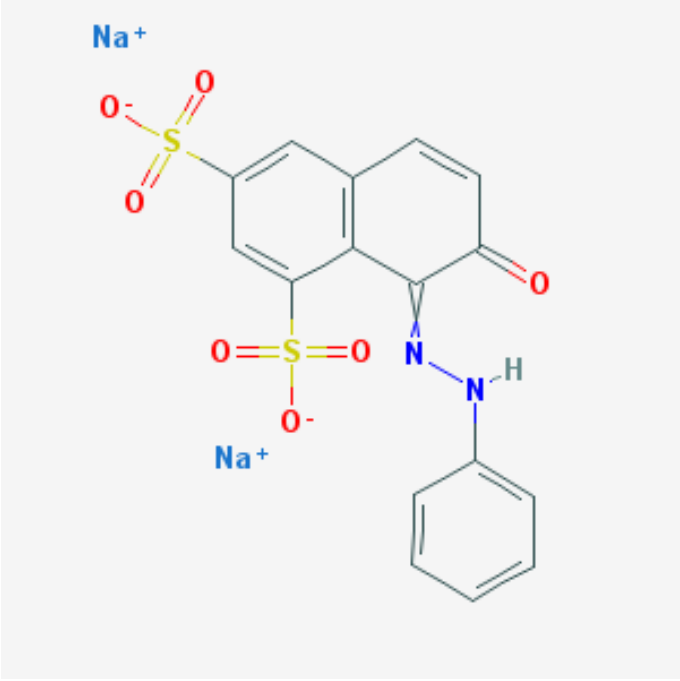

Figure 3.3 Molecular structure of Orange G and Sodium disassociation leading to a net negative two charge.

CHAPTER 4: **CHIP DESIGN AND FABRICATION**

The next part of this thesis was to create a paper microfluidic chip that could support electrophoreses based on the past works on paper electrophoresis and LFAs. Once the chip was designed, a fabrication protocol was formed to manufacture the chips using the materials selected previously. Flow times through the chips were measured for theoretical predictions needed in future sections.

4.1 Chip Design

The design of a microfluidic chip defines its function. For this thesis, the design of the microfluidic chip needed to incorporate an electrophoretic zone and separation channels to allow for the isolation of a dye. The sections of the chip that are found in most microPADs are the sample region, wick areas, and the channels. The sample region is a circular area where the sample is added to the chip. The wick areas provide extra volume to maintain fluid flow. Finally, the channels link the different regions of the device. The area that will differ from common microPADs is the electrophoretic zone where the sample separation takes place as well as a bifurcation of the channel into two channels, to keep the sample from re- mixing.

A sample is first introduced to the device on the sample area. The sample is absorbed into the cellulose paper fibers and capillary action transports the sample through the device. From the sample area, the fluid then enters the channel that transports it to the electrophoretic zone. Under the influence of an electric field, the sample separates based on charge and enters one of two channels separated by the bifurcation, keeping the separated sample from re-mixing. The sample will continue to flow down the channels

until it reaches the wicking area. Figure 4.1 shows sample flow through the device. Before separation occurs, the sample must complete the circuit between the electrodes located on both sides of the device in the electrophoretic zone. Once the circuit is completed, some of the dye will have to travel farther if it is on the transverse edge or have less time to separate to the correct channel if it is on the longitudinal edge. The importance of the initial condition will be discussed in future sections.

Figure 4.2 shows the fluid route and separation of the dye into different channels during steady state. Steady state is reached once the entire electrophoretic region has been saturated with the sample fluid.

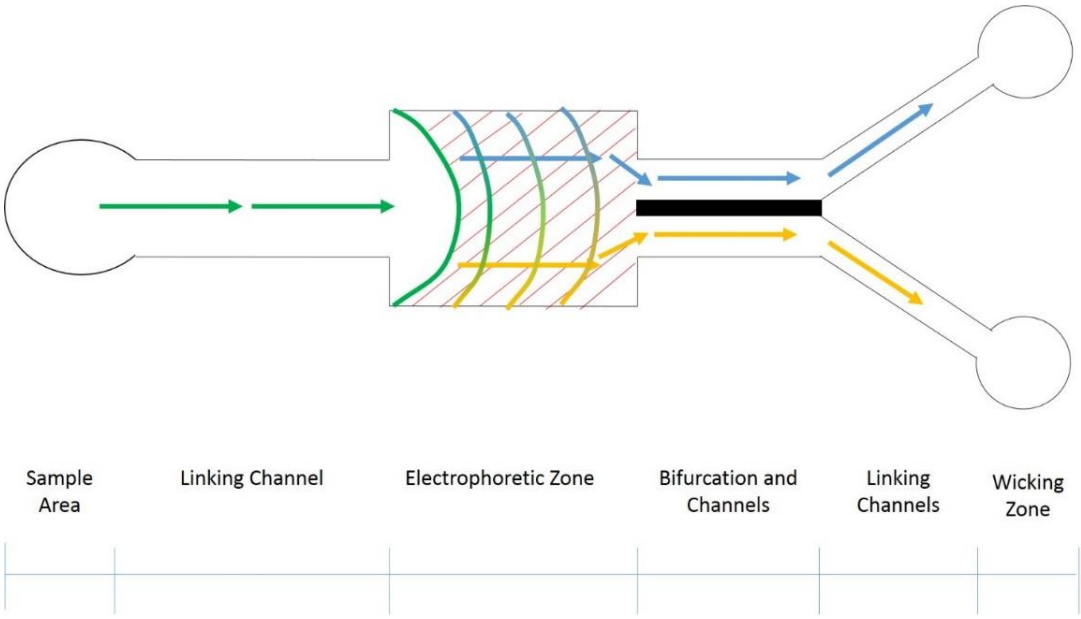

Figure 4.1 Initial condition before mixed solution (green) completes electric circuit (Red lines) and separates into different channels based on charge (blue and yellow). Curved lines show the progress of the fluid over time.

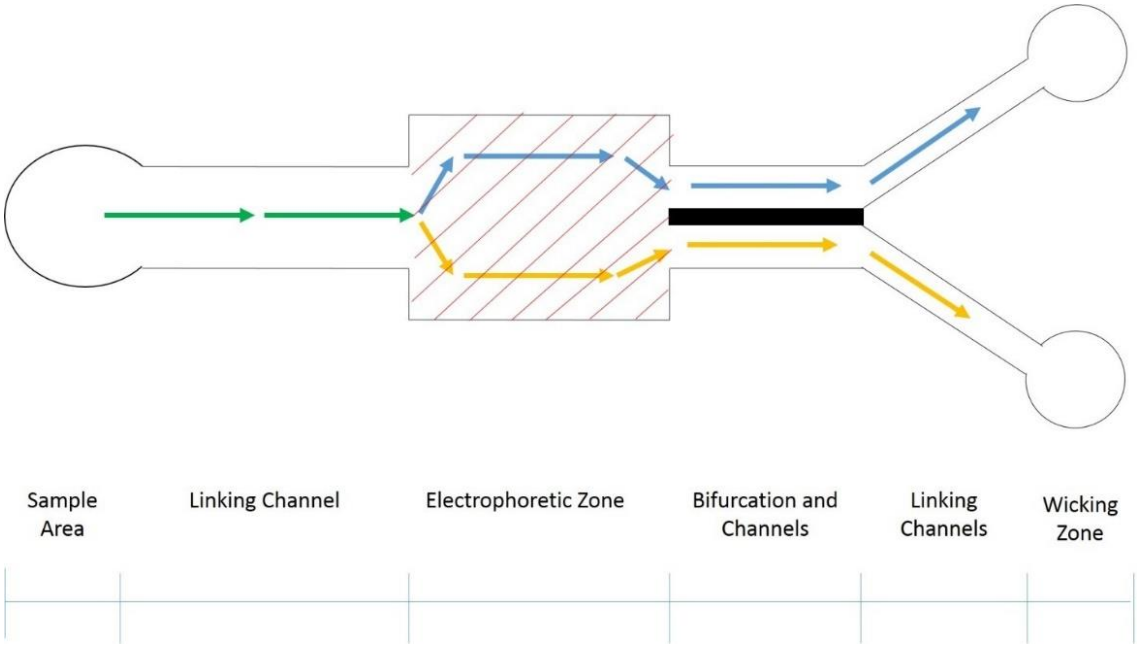

Figure 4.2 Drawing of a steady state condition in a microfluidic device with labeled sections and fluid routing path.

The final chip design that was used for the validation of the drift velocity theory consisted of all the components mentioned above. The outer dimensions of the chip had a 6 cm length and a 5 cm width. The sample area had a 0.5 cm radius with a 0.7 cm by 0.2 cm linking channel. The linking channel connected to the electrophoretic zone which measured 0.5 by 0.5 cm. The flow channel up until bifurcation had a dimension of 1 cm by 0.2 cm. Linking channels measured 1cm by 0.2 cm followed by the wicking zones with a 0.5 cm radius. A Cad drawing of the device can be found in Appendix B.2. Electrodes were applied to the edges of the electrophoretic zone using the conductive graphite described in earlier sections.

4.2 Chip Fabrication

In order to fabricate the microPADs, designs were first created using AutoCAD (Autodesk Inc). The designs were then transferred to cellulose paper using a PhotoCube wax printer (Xerox). Since the wax from the printer does not penetrate through the complete thickness of the membrane during normal printing, it was necessary to bake the printed wax membrane for about 30 seconds at 100°c using a heated plate (C-Mag HS 10, IKA). See Figure 4.3 below. After baking, the colloidal graphite electrodes were painted onto the chips so that the electric field could bypass the wax. The graphite paste was too thick to be used right from the container and needed to be thinned out using the Pelco graphite extender. Once the graphite was applied, it took about an hour to dry. In order to get clean lines and protect the channels from the graphite, tape was used to cover the channels that did not need the graphite before painting the graphite on the chips. Care was taken when painting to prevent smears and extra graphite from blocking the channels. The tape was carefully removed right after painting. See Appendix A.2 for the detailed chip fabrication protocol.

The creation of a paper chip was successful, and good microPADs were attained with the methods described above. The AutoCad software proved to be a good platform to create paper chips. The ability to change line widths, fill areas, create layers, and create complex shapes with ease made AutoCad a well-suited software for the design of paper chips. Printing the chips from the software was fairly straight forward.

Clean channel lines were possible with the wax printer, and it allowed for the rapid creation of many paper chips in a single run. Figure 4.3 shows the wax printer and

multiple chips after being printed. The dark area is wax deposited by the printer. The hot plate that was used to melt the wax into the cellulose membrane and the resulting chip is also shown in Figure 4.3. After baking the chips, the wax changed color from black to gray as the wax penetrated the paper. Only a small amount of spreading from the original dimensions was observed after baking. The only drawback was the occasional paper jam that would ruin the paper, which required starting the process from the beginning.

The graphite paste that was selected also worked well. The paste was applied to the paper with the brush that came with it and had good adhesion to the paper and wax. Although the paste was too thick to use straight from the bottle, by using the extender the correct consistency was made. Compared to the other options, the colloidal graphite was better in ease-of-use and cost. The main problem with the graphite was that it would flake and chip away if too much bending in the paper occurred. If a large amount of the graphite chipped away, then the circuit would break. If the graphite did chip away, it was easy to repair by scraping off the remaining graphite and applying another layer.

Figure 4.3 PhotoQube wax printer (top left) heating plate (top Right) cellulose paper with printed autocad design pre-baking (bottom left) and cellulose paper with autocad design post-baking (bottom right).

4.3 Chip Flow Times

To predict the required electric field to cause separation of a sample, it was necessary to create an equation using the amount of time the dye takes to enter and leave the electric field. Since the sample flow was in the longitudinal direction, perpendicular to the electric field, it was not directly affected by the electric field. To measure the average time it takes for the sample to pass the electric field, ten chips were run, five with 10 mM and five with 1 mM OG dye. The times were measured by recording the separations using a Nexus 5 cell phone camera (LG). Time was started as soon as the dye entered the electrophoretic region and was stopped when the dye reached the end of the channel. The time when the dye made contact with the walls of the channel was also recorded. This time corresponds to when the dye would make contact with the electrodes and enter into the initial condition flow.

The run times through the electrophoretic zone were similar for both 1 mM and 10 mM dyes. The average time in the electrophoretic zone for 1 mM was 41.9±0.1 seconds and for 10 mM was 43.8±0.1 seconds. The average total time for 1 mM and 10 mM was 55.8±0.1 and 57.7±0.1 seconds, respectively. The shortest time that was recorded in the electrophoretic zone was 39.6±0.1 seconds for 1mM and 37.3±0.1 seconds for 10 mM. The shortest total time for 1mM and 10mM concentrations was 53.0 ±0.1 and 50.2 ±0.1 seconds, respectively. Table 4.1 shows the recorded flow times

described above, and Appendix C.1 contains the raw data for the chip flow times. The flow rates measured were faster than what was claimed by the company. The measured average flow rate for the channel was 159/30 mm/min for the grade 1 chromatography paper but was advertised to have a flow rate of 130/30 mm/min.

Table 4.1 Flow Times through Electropheretic Zones for 1 mM and 10 mM Dye.

Concentration	Average Time in Electrophoretic zone(s)	Average Total Time(s)	Shortest time in Electrophoretic Zone(s)	Shortest Total Time(s)
1 mM	41.9±0.1	55.8±0.1	39.6±0.1	53.0±0.1
10 mM	43.8±0.1	57.7±0.1	37.3±0.1	50.2±0.1
1 & 10 mM	42.8±0.1	56.7±0.1	37.3±0.1	50.2±0.1

CHAPTER 5: **DRIFT VELOCITY**

5.1 Introduction

The next step in this thesis was to characterize the electrophoretic separations on cellulose paper. Predicting separation speeds on cellulose paper presented many problems. Membrane materials have a complex structure of fibers that create a network of pathways for fluids to flow through. Due to the high volume fraction of cellulose fibers, it was expected that the fibers would cause significant hindrance of the movement of particles through the paper. Properties for fibrous materials have been predicted previously using computer models; however they have been based on uniform packing arrangements such as face centered cubic (FCC) or body centered cubic (BCC) lattices. Since cellulose membranes do not have a regular packing structure, the properties are only estimates for cellulose membranes.

There are many corrections for fluid flow in a fibrous medium. In this paper, we will estimate hindrance caused by cellulose fibers using the Brinkman correction. This correction only holds true at low volume fractions. Since the volume fraction of the cellulose membrane used for this experiment is high, the correction may lose validity but can still provide a rough estimate of separation speeds. Since the correction does not take into account sample concentration, effects of two dye concentrations were tested.

Cellulose paper chips created and fabricated using the methods from the previous chapter were used to measure separations speeds. Separation speeds were measured visually by direct recording of dye in an electric field with a camera. Steps were taken to

reduce the amount of forces caused by membrane-fluid interactions to isolate the electrophoretic force.

5.2 Electrophoretic Velocity Measurements

The velocity of the conductive dye Orange G in a given electric fielded needed to be quantified before a chip could be used to separate the dye into separate channels. The setup used two reservoirs, one filled with a solution of O.G. dye and the other filled with water. Then, by bridging the two reservoirs with cellulose, the dye could be pulled across to the other reservoir. To move the dye, an electric gradient was applied to the reservoirs. Since the dye is negatively charged, the reservoir without the dye was connected to the positive electrode. Once the gradient was established, the dye particles were attracted to the positive electrode and flowed through the membrane. By setting up a ruler next to the chip and taking video recordings, separation velocities were measured. Experimental set-up is shown in Figure 5.1 and described below.

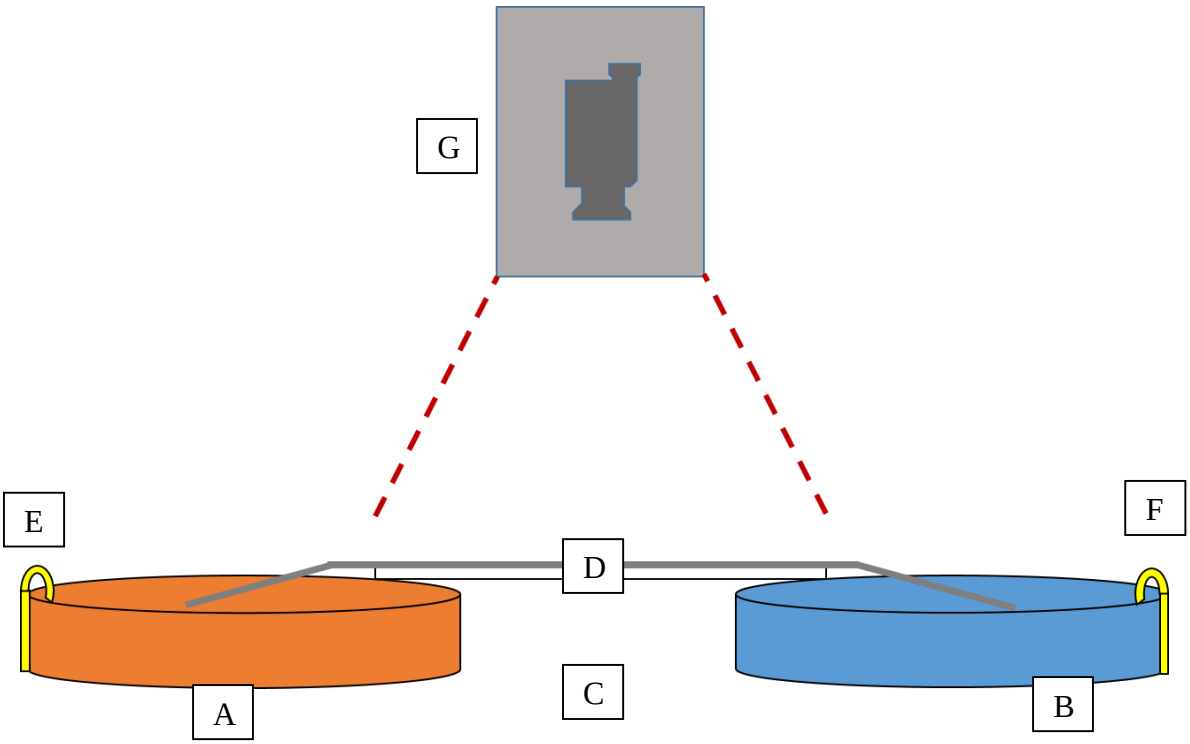

Figure 5.1 Concept of experimental setup for drift velocity measurements. (A) Reservoir with O.G. dye (B) Reservoir with water (C) Platform to hold cellulose membrane (D) Cellulose membrane (E) Negative electrode (F) Positive electrode (G) Recording device to make videos of separations for velocity measurements.

To define the electric field, a simple chip was created using the chip fabrication methods described previously. The chip consists of a channel 6 mm wide by 14 cm long and was open at the ends to allow fluid transfer. The purpose of this experiment was to define the velocity of the dye caused solely by the electric field; other interactions, most notably capillary action, that effect velocity needed to be suppressed. To accomplish this, the chip was pre-saturated with tap water since the high ion content gave it excellent conductivity to conduct the electric field across the length of the chip. Other purified waters, such as deionized or distilled water, have high resistivity resulting in poor conduction of an electric field.

After the chip was saturated, it was placed on a glass slide that was smaller in length than the channel so the strips were hanging over the ends of the glass slide. The glass slide and the channel were placed on top of two petri dishes. One petri dish contained the Orange G solution with a concentration of either 10 mM or 1 mM, and the other petri dish contained tap water. The petri dishes were connected to a LabSmith high voltage sequencer power supply (HVS448 3000V, LabSmith Inc) using alligator clips set at a distance of 20 cm apart with a ruler aligned next to the channel. Next, voltage was applied from the power supply at 0, 50, 100, 150, and 200 V, and the electric field would pull the dye through the chip toward the petri dish with tap water. While the experiment was running, the dye movement was recorded using a video camera. From the video, distances traveled by the dye in a given time frame could be measured using the ruler and drift velocities were determined.

Drift velocities were analyzed based on the time the dye took to travel one centimeter. The starting point was defined by the dye reaching the tick mark on the ruler marked as zero. The end of the measurement was the one centimeter mark. The drift velocity protocol can be seen in Appendix A.3.

Figure 5.2 LabSmith high voltage sequencer used to apply voltage to devices (left) and experimental set up (right).

5.3 Results

5.3.1 Theoretical Calculations

Drift velocity values were calculated using Eq. (7) derived previously. The values were used to compare velocities attained experimentally as described above. The electric field strengths used experimentally were 0, 250, 750, and 1000 volts/meter. Sample calculations comparing theoretical and experimental values are shown below for E-field strength of 1000 volts/meter. The sample calculations are broken into three parts: (1) electro-kinetic attraction (2) Stoke's drag, and (3) Brinkman correction. The three steps solve for velocity using Eq. (7).

(1) The electro-kinetic attraction is defined by the charge of the particle, in this case the O.G. dye, which has a charge of -3.204 E-19 Coulombs and is multiplied by the electric field strength of 1000 Volts/meter.

$$qE_x$$

3.204 E-19 C x 1000 volts/meter

$$qE_x\text{=3.2E-16 }\frac{C*volts}{meter}$$

(2) The hydrodynamic resistance, or Stoke's drag, is calculated using the particles radius that was found in Chapter 2 and the viscosity of the water as an estimate for the dye's viscosity.

$$\xi = 6\pi a\mu$$

6 * π * 0.54E-9 m * 0.00091 kg /m*s

$$\xi = \text{9.26267E-12}\frac{kg}{s}$$

(3) The Brinkman correction to Stoke's drag takes into consideration the radius of the matrix fibers measured in Chapter 2 to be 14.6 μm and the membrane porosity. Membrane porosity values can normally be found on data sheets provided by the vendor where the membrane was purchased; however, the membrane data sheet used in this thesis did not supply that value. Since the membrane porosity of the cellulose could not be found, results from a computer model by Higdon and Ford was used to estimate a value [30]. By estimating a volume fraction of 0.6, using the fiber radius for the cellulose membrane, and a BCC fiber packing orientation, a brinkman screening length of 718281 m^{-1} was found.

$$(1+\propto \mathrm{a}_f + \frac{(\propto \mathrm{a}_f)^2}{3})$$

$$1 + 718281 * 1.08\text{E-}09 + \frac{(718281 * 1.08\text{E}-09)^2}{3}$$

$$1.000936534$$

By combining (1), (2), and (3) back into Eq. (7) the result is:

$$u_E = \frac{3.2\text{E}-16 \frac{C*volts}{meter}}{\left(9.26267\text{E}-12 \frac{kg}{s}\right)*1.000936534}$$

u_E=0.00345781 m/s or 2.07 mm/min

Table 5.1 O.G. Theoretical Drift Velocity Results.

Electric Field strength(v/m)	250	500	750	1000
O.G Theoretical Drift Velocity (mm/min)	0.52	1.04	1.56	2.07

5.3.2 Drift Velocities Compared to Theory

Theory predicts the velocity based on a change in electric field strength. The four field strengths used were 250, 500, 750, and 1000 volts/meter and theory predicts a velocity of 0.52, 1.04, 1.56, and 2.07 mm/min respectively. An electric field of zero was used to normalize the values by subtracting the zero speeds and eliminating any impact on velocity not attributed to the electric field. The 1 mM O.G. experimental velocities were on average faster than the theoretical values. The average velocities for 1 mM O.G. were 0.57±0.04, 1.13±0.10, 1.56±0.11, and 2.20±0.15 mm/min, and for 10 mM O.G. the average velocities were 0.59±0.08, 1.38±0.09, 1.79±0.14, 2.45±0.10 mm/min with increasing electric field strength. For both concentrations there was a significant

difference in velocity for different electric field strengths with $p<0.05$. Comparing the same voltage but at different concentration showed no significant difference at any electric field strength with $p>0.05$. The data described above is summarized using the bar chart shown below in Figure 5.3. All statistics were performed using Minitab statistical software (Minitab Inc) and statistical output is shown in Appendix C.3.

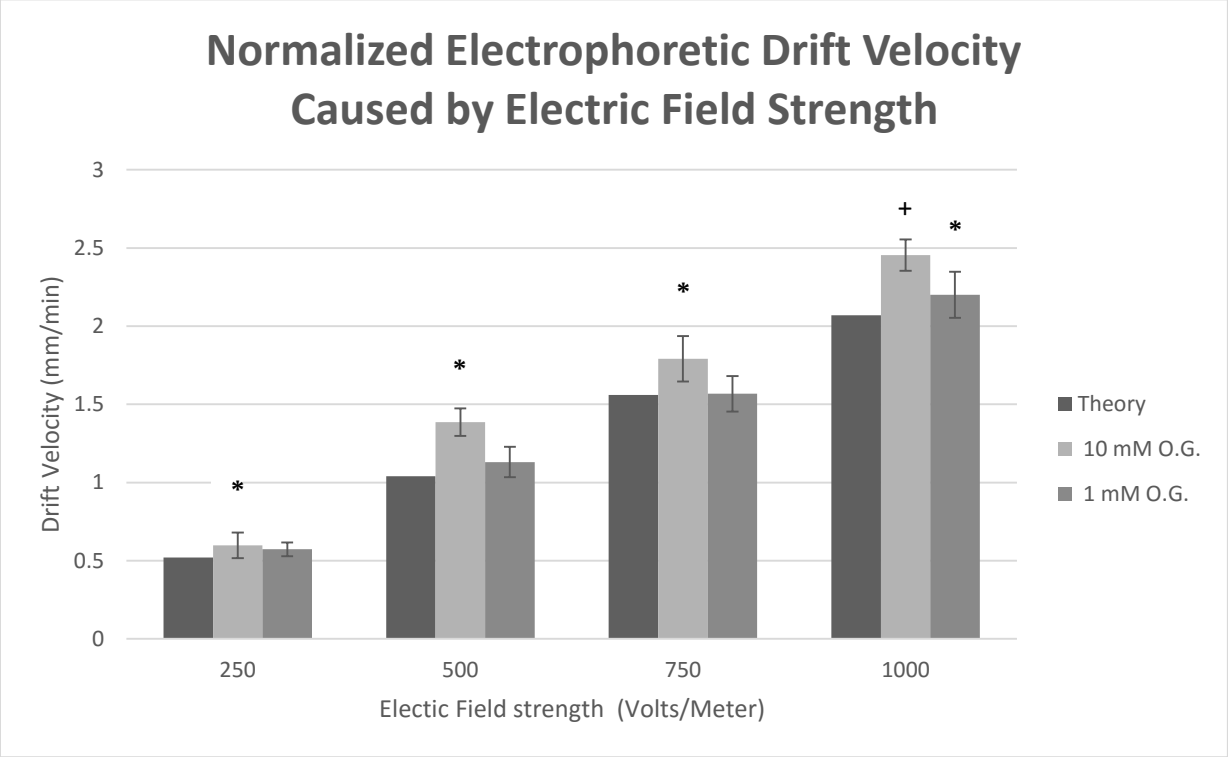

Figure 5.3 Normalized drift velocities for OG conductive dye at 1mM and 10 mM concentration compared to theory. For 1mM concentration there was a significant difference between each voltage the group and 10 mM was the same (* $P<0.05$). Comparing the same voltages for different concentrations showed only at 200V there was a difference in velocity (+$P<0.05$).

Next, the averages of the velocities were plotted and fitted with a linear regression line and is shown Figure 5.4. The regression of 1 mM O.G. gave the equation Velocity = 0.0021V + 0.0382 with an R^2 of 99.55%, the 10 mM O.G. regression gave Velocity = 0.0024V+ 0.0644 with an R^2 of 98.64%. The theoretical predication gave a

linear regression of Velocity = 0.002V- 0.001, which is close to the measured values, just slightly lower.

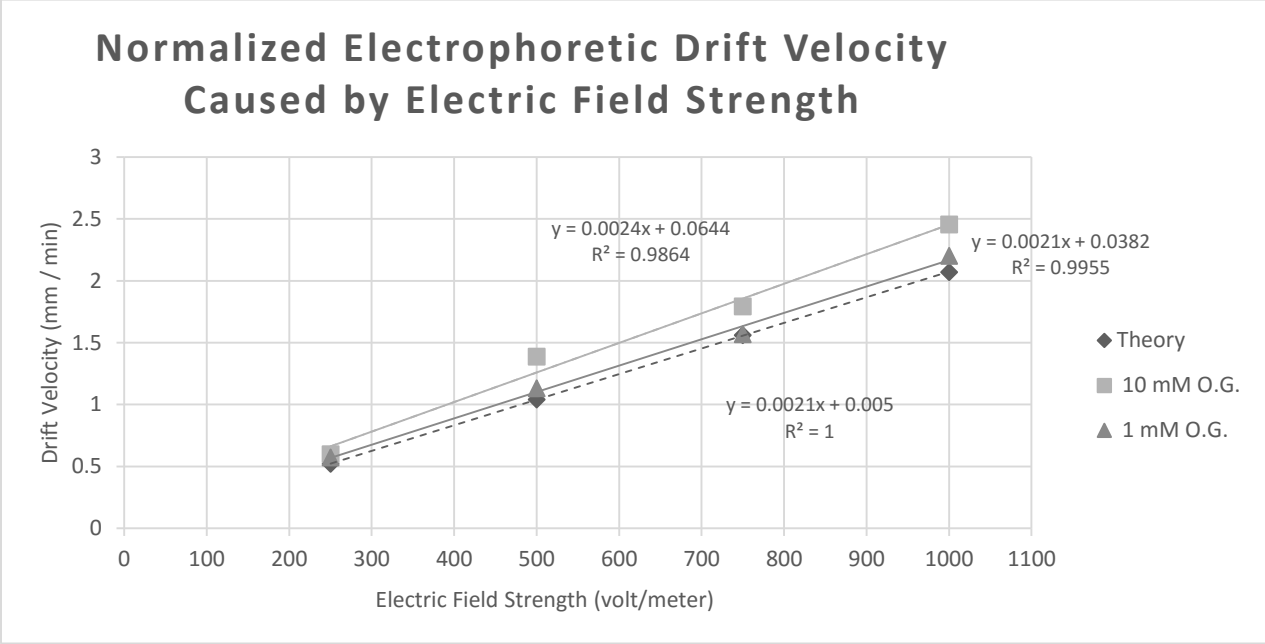

Figure 5.4 Plot of normalized average velocities for Theory, 1 and 10 mM OG fitted with a linear regression.

CHAPTER 6: **VELOCITY VALIDATION**

6.1 Introduction

Chapters 4 and 5 provided the necessary information for applying electrophoresis to a paper microfluidic device. Chapter 4 described the process of creating a fabrication protocol and a chip design that allows electrophoresis. Chapter 5 compared the experimental values to theory to determine drift velocity through the chosen cellulose membrane. With the information attained in these chapters, the drift velocities could then be predicted for the cellulose chips.

In this chapter, the theory will be modified from the chip in the previous chapter, which attempted to eliminate fluid flow caused by factors other than the electric field, and applied to a small electrophoretic zone. The chip in this chapter will utilize capillary action as the main driving force for fluid transportation and leverage electrophoresis as a secondary force applied transverse to capillary flow to separate particles into different channels.

6.2 Methods

6.2.1 Validation of Electrophoretic Velocity Measurements

The next part of this thesis was to validate the separation velocity that was measured in previous sections and use an electric field to separate a colormetric die on a microPAD. The validation was performed by creating 2D wax paper microfluidic chips that have a transverse electric field applied. Using the velocity measurements that were taken in previous sections, the amount of time the dye is under the influence of the electric field, and distance the dye has to travel, an equation was created based on theory

to predict the necessary voltage to successfully separate the dye. Then using the results of the velocity measurements, a linear regression of the data was used to create an equation based on experimental data to predict the voltage required to separate the conductive dye. These equations are shown in Figure 5.4.

Validation of the drift velocity regression was performed by attempting to separate the O.G. dye in a transverse electric field. If the equations found previously could successfully predict the applied voltage required to cause separation, the equations would be considered valid. To perform the validation, a microfluidic chip capable of preforming transverse electrophoreses was created as described in Chapter 4.

6.2.2 Transverse Separations

Using the chip mentioned above and applying the equations derived and found experimentally to the dimensions of the chip, separation voltage could be predicted. From theory, Eq. (10) predicts the required voltage for dye separation. The last value needed was the time for the solution to completely cross the electrophoretic zone. This was averaged over five experiments and measured to be 54.8 seconds. This speed is important to know since faster fluid flow times require stronger electric fields to separate the particles before they cross the electrophoretic zone. With this in mind, rather than using the average fluid flow time, the fastest time was chosen, 50.2 seconds, in order to assure that successful separation with every experimental run. Additionally, 12.9 seconds, the time required for the fluid to reach the electrophoretic zone, was subtracted from the total time, resulting in a final fluid flow time of 37.3 seconds. The transverse velocity required was calculated by dividing the electrophoretic longitudinal flow time by

the electrophoretic channel width of 5 mm giving a minimum required velocity of 8.03 mm/min for the initial condition and a velocity of 3.58 mm/min at steady state.

Next, by applying the material properties of the membrane, the dimensions of the channel, and the crossing time of the fluid, the theoretical voltage can be found. By setting the drift velocity equal to 0.62 mm/min, the applied voltage required to attain the drift velocity can be calculated.

The first step is to calculate the hydrodynamic drag with the Brinkman correction:

$$c_{Brink} = (1+\propto \mathrm{a}_f + \frac{(\propto \mathrm{a}_f)^2}{3})$$

$$c_{Brink} = (1 + (5\mathrm{E} - 10 * 8.80\mathrm{E}5) + \frac{(5.0\mathrm{E}-10*8.80\mathrm{E}5)^2}{3})$$

$$c_{Brink} = 1.000444$$

$$\xi = 6 * 3.14 * (5E - 10\ m) * \left(1E - 3\ \frac{N * s}{m^2}\right) * 1.000444$$

$$\xi = 9.43\mathrm{E} - 12\frac{N * s}{m}$$

Now substitute into Eq. (10) and solve:

$$Vap = \frac{\delta_T \delta_E 6\pi a\mu\ (1+\propto a + \frac{(\propto a)^2}{3})}{q}$$

$$\mathbf{V_t} = \frac{\left(\mathbf{0.000134}\frac{\boldsymbol{m}}{\boldsymbol{s}}\right) * (\mathbf{0.005}\ \boldsymbol{m}) * (\mathbf{1.07E}\frac{\boldsymbol{N * s}}{\boldsymbol{m}})}{\mathbf{3.20435314}\boldsymbol{E} - \mathbf{19}\ \boldsymbol{C}}$$

$$Vap = 20.09 \text{ V}$$

Theory predicts that an applied voltage of 20.09 volts for the dimensions of the channel is sufficient for particle separation using an O.G. dye solution. From the linear regression equations, the applied velocity can also be estimated. The linear regression of the 10 mM O.G. was y = 0.0024x - 0.0644 and for 1 mM O.G. the equation was y=0.0021x - 0.0382, from Figure 5.4. The equations predict drift velocity given an applied electric field. By rearranging and solving for x, the electric field strength required to attain the velocity can be found. In order to convert the electric field strength to the applied voltage on the microfluidic chip, the voltage needs to be multiplied by the distance between electrodes. A sample transformation is shown below for the 1 mM O.G. equation.

$$\text{y} = 0.0021\text{x} + 0.0382$$

$$\frac{\text{y} - 0.0382}{0.0021} = \text{x}$$

$$\text{x} = (476.2\text{y} - 018.2) * (0.005)$$

$$\text{x} = 2.4\text{y} - 0.09$$

The resulting equations from the transformations gave $x = 2.4y - 0.09$ and $x = 2.1y + 0.13$ for 1mM and 10mM O.G. respectively. Using the equations above and substituting the velocities calculated previously, the required applied voltages for initial state and steady state can be found in Table 6.1. For this thesis, the predictions would be considered successful if the voltages could route the dye into a single channel without appearing in the other channel six times. If the dye did not completely separate into a

single channel, then the calculated voltages would be considered inadequate. The voltage and current for each trial was recorded in Appendix C.4. Current was recorded to track information on jewel heating, which could be a factor resulting in evaporation of the fluid.

Table 6.1 Required voltages for separation velocities for 1 and 10 mM OG dye at initial state and steady state.

Name	Applied Voltage Initial	Applied Voltage Steady
Theory	20.09	8.95
10 mM	16.60	7.32
1 mM	19.04	8.43

6.3 Results

Using the voltages calculated in Table 6.1, the separations on the paper chip were attempted. When 1mM O.G. dye was used, the separations where successful six out of six attempts. When 10 mM O.G. dye was used, the voltages failed to separate the dye the first three attempts, and therefore no further attempts were tried. Figure 6.1 shows results at steady state with 1 mM and 10 mM O.G. trials. The separation is clearly seen in the 1 mM chip with the dye showing a digagonal path to the right hand channel. The 10 mM chip shows little movement of dye, only slightly in the left hand electrophoretic zone.

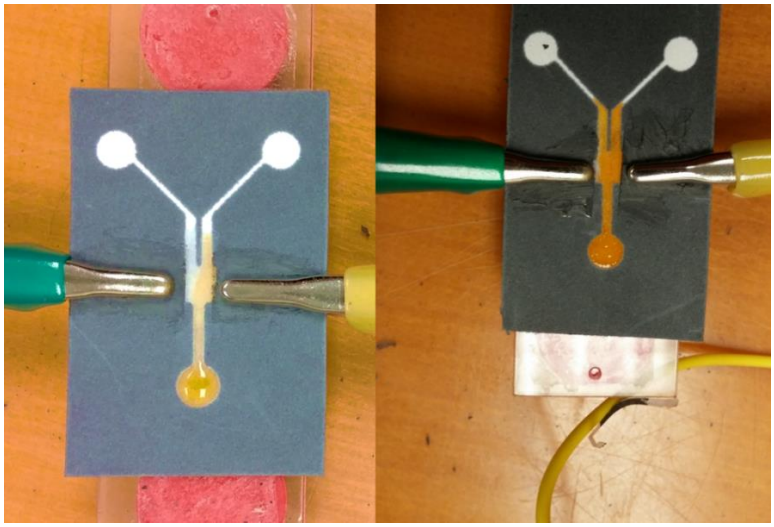

Figure 6.1 Successful separation of 1 mM O.G. dye (left) and unsuccessful separation of 10 mM O.G. dye (right).

During each experiment the voltage and current traces were recorded from the voltage sequencer program. The voltage plots were similar for all trials. Two examples can be seen in Figure 6.2 and Figure 6.3. The blue lines represent the calculated required voltages supplied to the sequencer. In Figure 6.2, traces of applied voltage and current can be seen for 1 mM O.G. dye separation trial and the drop in current from initial condition (19 V) to steady state (8 V) is clearly seen. In both images, the resultant current that was applied across the chip varied with time. During the initial condition, the applied current increased to a maximum of about 60 uA. When the voltage dropped with the onset of steady state, the current dropped as well. After the current drop, both images demonstrate a rising current for a period of time and after begin their downward trend until the end of the experiment. Across trials, the current levels followed the same similar trend except that the maximum and minimum levels varied, as well as the time

point when the current slope began trending downward. All trace graphs can be found in Appendix C.4.

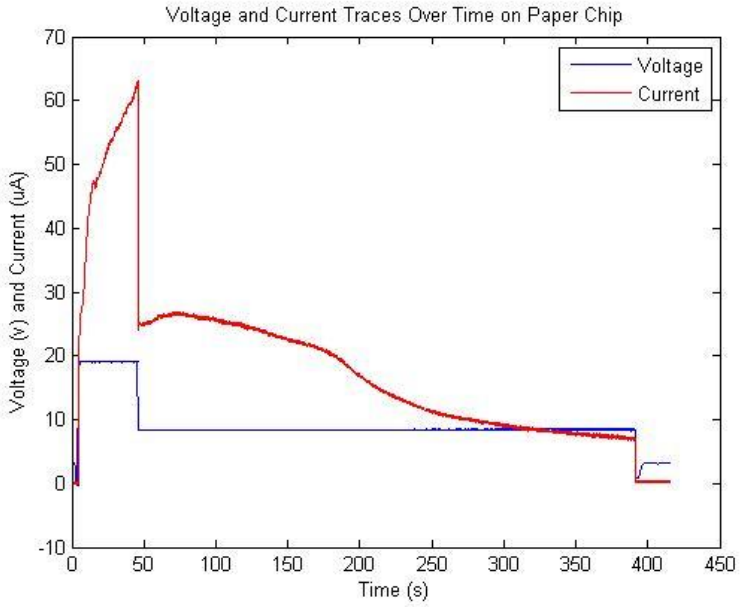

Figure 6.2 Traces of the applied voltage (blue) and the resultant current (red) during a 1 mM O.G. dye separation on a paper microfluidic chip.

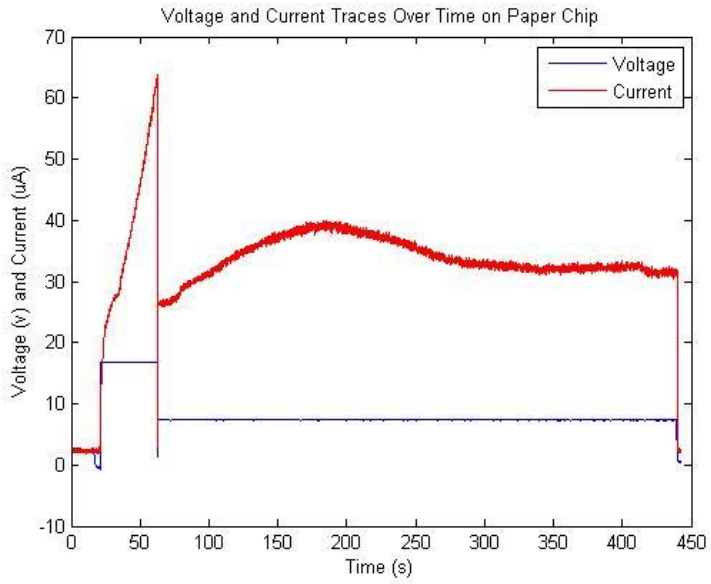

Figure 6.3 Traces of the applied voltage (blue) and the resultant current (red) during a 10 mM O.G. dye separation on a paper microfluidic chip.

CHAPTER 7: **CONCLUSIONS**

7.1 Incorporation of Electrophoresis

The results presented in this thesis indicate that the fabrication of paper chips that can support the application of an electric gradient is possible. Furthermore, the materials needed are minimal and most can be purchased at on office supply store such as the printer, scissors, and tape. The only materials that would be more difficult to find would be the chromatography paper and the colloidal graphite paste. Although the addition of electrophoretic capabilities to a microPAD increases the complexity of the chip and leads to a greater fabrication time and overall cost, the increases are small.

The only difference in terms of fabrication from a microPAD that does support an electrical gradient and a microPAD that does not is the electrode material. The

complexity that is added by the chip design in order to support electrophoresis has almost no effect on fabrication because the printer has the capabilities to print almost any design. However, application of the electrodes does add a new step in fabrication, which adds a significant time increase in manufacturing. The time increase is large for two reasons: first, the electrodes are applied to the device by hand, and second, the electrodes have to dry before use. Both these time delays can be reduced by an automation process for the application of the electrodes and decrease drying time of the electrodes by drying them at a warmer temperature.

7.2 Predicting Electrophoretic Separation

The results from the Figure 5.3 show that the measured velocities for both concentrations of dye are faster than what theory predicts. However, the theoretical values are still close to experimental data and is a good predictor of separation velocity in the electric field range used. At higher electric field values, the theoretical and experimental values seem to drift apart, especially for the 10 mM concentration O.G. dye.

7.3 Verification of Electrophoretic Separations

The separation of O.G. dye worked well at 1 mM concentration but poorly at 10 mM. It is clear from both images seen in Figure 6.1 that the dye enters and crosses the electrophoretic zone and then exits the electrophoretic zone into the exit channels. The results show that theory can predict the voltages required for separation and provides a repeatable platform, however, there are some limitations present.

A possible explanation for why the 10 mM dye did not separate can be a result of the increased concentration of the charged dye applying repulsion forces. Since the dye is

charged, it will repel like-charged particles such as itself. At lower concentrations, this repulsion force is smaller whereas at higher concentrations the force may be stronger and repel against the electric field that is trying to bring them together.

In summary, the paper chip created was successful in separating O.G. dye into bifurcated channels using the voltages that were calculated from the results of Chapter 4 for the 1 mM O.G. dye. Even though the separation of the 10 mM O.G. dye was unsuccessful, it is considered a problem with the dye concentration and not the experimental setup. The results are considered successful and have shown promise for the future of this technology.

7.4 Future Work

The application of electrophoresis on microPADs is a promising addition to paper microfluidics. However, there are more applications that need to be explored further. Future work can apply electrophoresis to isolated multiple targets or filter out unwanted particles using the isoelectric separation. Another modification could be to change the shape of the chip or electrophoretic zone to cater to individual testing needs.

7.4.1 Integration of Electrophoretic Separation with Lateral Flow Assay

Now that the application of electrophoretic separations on microfluidic paper chips has been shown possible, the next step is to apply an electrophoretic separation for a biological detection. The placement of the separation zone is as important to perform the separation early in the chip when sample volume is high and flow times are fast. In most cases it seems that the separation should occur before the conjugate zone where the material changes to a woven mesh or nitrocellulose in the detection region. It may be

possible to apply separations on chips that currently do not use impregnated hydrophobic barriers by adding electrodes and cutting out a channel bifurcation. The integration of electrophoresis in paper chips has the potential to make chips more accurate and useful.

7.4.2 Electrophoretic Zone Modifications

One aspect of the design of the chip that was not experimented with in this thesis is the electrophoretic zone shape. This thesis tested a simple rectangle design. By changing the shape of the electrophoretic zone, different properties can be created. For example, the rectangular design used in this thesis required a two-stage voltage application for efficient separation; however, by changing the shape to a conical design, it could eliminate the need for a two-stage voltage application. Other design options include a semi-circle, triangular, or trapezoidal shape. Novel shapes could be created using a combination of designs for separating complex mixtures.

Still, using complicated designs for the electrophoretic wall has some draw backs. Since the distance between the electrodes will vary, the electric field strength will vary as well. This causes a gradient-dependent separation velocity as a particle passes through the electric field. To calculate the required applied voltage, it is necessary to take the required field strength and multiply it by the average distance between the electrodes. This may be beneficial since separation speeds can be altered by changing the distance between the electrodes without the need to modify voltage.

7.4.3 Multiple Targets

Detecting multiple targets in a sample is one of the advantages microPADs could offer [31]. By using electrophoresis, particles can be separated by charge and diverted

into different channels. The simplest method would be to separate positive, negative, and neutral charges. Figure 7.1 shows an example of what a microfluidic device with electrophoretic separation might look like. The beginning of the chip looks and functions the same as the chip tested in this thesis; however, instead of dividing into two channels, the channel splits into three. Each of these channels contain a typical lateral flow assay. Each LFA can test for a different target. At the end, the channels come back together into the wicking pad. More advanced devices may separate particles based on how strong the charge of a molecule is and the size of the target. Additionally, depending on the channels, different assays could be performed based on what is expected to be found for each charge.

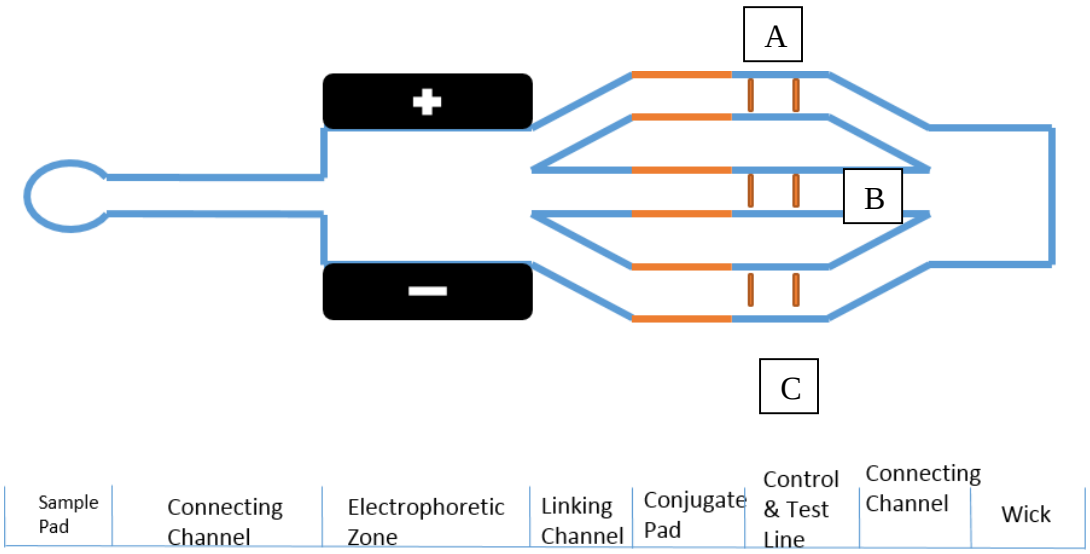

Figure 7.1 Example of how an electrophoretic separation may be used with a paper chip. Uses three channels to separate particles by positive (C), negative (A) and neutral charges (B).

7.4.4 Isoelectric Separations

The ability to isolate one target in a solution using minimal equipment is often the goal of microPADs. This means that these devices should try and use raw samples without purification. Using an isoelectric separation, purification could occur on the device with minimal equipment. An isoelectric point is the point at which a charged particle in a given particular pH renders the effective charge of a molecule to zero [32]. This allows a molecule to pass through an electric field unaffected while undesirable molecules can be filtered into different channels. This can also be performed on different types of biologicals. For example, bacteria have a surface charge, and this technique can isolate specific types of bacteria [33]. The ability to remove unwanted waste and isolating a single target may help these devices to work with raw samples.

REFERENCES

1. Martinez, A.W., et al., *Diagnostics for the developing world: microfluidic paper-based analytical devices.* Anal Chem, 2010. 82(1): p. 3-10.
2. Mandal, P., R. Dey, and S. Chakraborty, *Electrokinetics with "paper-and-pencil" devices.* Lab Chip, 2012. 12(20): p. 4026-8.
3. Lu, Y., et al., *Fabrication and Characterization of Paper-Based Microfluidics Prepared in Nitrocellulose Membrane By Wax Printing.* Analytical Chemistry, 2009. 82(1): p. 329-335.
4. CDC, *Global Disease Detection Program*. 2010: Atlanta.
5. W.H.O., *Accessible quality-assured diagnostics*. 2008, World Health Organization. p. 32.
6. Block, R.J., E.L. Durrum, and G. Zweig, *A manual of paper chromatography and paper electrophoresis*. 1958: Academic Press (New York). 710.
7. Köiw, E. and A. Gröwwall, *Staining of Protein-Bound Carbohydrates after Electrophoresis of Serum on Filter Paper.* Scandinavian Journal of Clinical & Laboratory Investigation, 1952. 4(3): p. 244-246.
8. Aronsson, T. and A. Grönwall, *Improved Separation of Serum Proteins in Paper Electrophoresis — A New Electrophoresis Buffer.* Scandinavian Journal of Clinical & Laboratory Investigation, 1957. 9(4): p. 338-341.
9. Westermeier, R. and S. Gronau, *Electrophoresis in practice : a guide to methods and applications of DNA and protein separations*. 4th rev. and enl. ed. 2005, Weinheim: Wiley-VCH. xx, 406 p.
10. Durrum, E.L., *A Microelectrophoretic and Microionophoretic Technique1*. Journal of the American Chemical Society, 1950. 72(7): p. 2943-2948.
11. Gordon, M.J., et al., *Capillary electrophoresis.* Science, 1988. 242: p. 224+.
12. National Institute of Higher Education, R., Science and Technology. *Microfluidics*. 5/30/13]; Available from: http://www.niherst.gov.tt/scipop/sci-bits/microfluidics.htm.
13. Gravesen, P., J. Branebjerg, and O.S. Jensen, *Microfluidics-a review.* Journal of Micromechanics and Microengineering, 1993. 3(4): p. 168.
14. Chin, C.D., V. Linder, and S.K. Sia, *Lab-on-a-chip devices for global health: past studies and future opportunities.* Lab Chip, 2007. 7(1): p. 41-57.
15. Millipore, *Rapid Lateral Flow Test Strips Considerations for Product Development*. 2008. p. 42.
16. Posthuma-Trumpie, G.A., J. Korf, and A. van Amerongen, *Lateral flow (immuno)assay: its strengths, weaknesses, opportunities and threats. A literature survey.* Anal Bioanal Chem, 2009. 393(2): p. 569-82.
17. Wong, R.C. and H.Y. Tse, *Lateral flow immunoassay*. 2009, New York, NY: Springer. xii, 223 p.
18. Carter, D.J. and R.B. Cary, *Lateral flow microarrays: a novel platform for rapid nucleic acid detection based on miniaturized lateral flow chromatography.* Nucleic Acids Res, 2007. 35(10): p. e74.
19. Buechler, K.F., et al., *Simultaneous detection of seven drugs of abuse by the Triage panel for drugs of abuse.* Clinical Chemistry, 1992. 38(9): p. 1678-84.

20. Pall, *Optimized, highly efficient membrane for one-step plasma separation from whole blood without the use of centrifugation*. 2000, pall: Ann Arbor. p. 6.
21. Erickson, D., D. Sinton, and D. Li, *Joule heating and heat transfer in poly(dimethylsiloxane) microfluidic systems.* Lab on a Chip, 2003. 3(3).
22. Nie, Z., et al., *Electrochemical sensing in paper-based microfluidic devices.* Lab Chip, 2010. 10(4): p. 477-83.
23. Dungchai, W., O. Chailapakul, and C.S. Henry, *Electrochemical detection for paper-based microfluidics.* Anal Chem, 2009. 81(14): p. 5821-6.
24. Duffy, D.C., et al., *Rapid Prototyping of Microfluidic Systems in Poly(dimethylsiloxane).* Analytical Chemistry, 1998. 70(23): p. 4974-4984.
25. Fournier, R.L., *Basic transport phenomena in biomedical engineering*. 2nd ed. 2007, New York: Taylor & Francis. xxii, 450 p.
26. Brinkman, H.C., *A calculation of the viscous force exerted by a flowing fluid on a dense swarm of particles.* Applied Scientific Research, 1949. 1(1): p. 27-34.
27. Lu, Y., et al., *Rapid prototyping of paper-based microfluidics with wax for low-cost, portable bioassay.* ELECTROPHORESIS, 2009. 30(9): p. 1497-1500.
28. Mehta, R., *Interactions, Imaging and Spectra in SEM.*
29. Sigma-Aldrich. *O3756 - Orange G.* 5/29/2013]; Available from: http://www.sigmaaldrich.com/catalog/product/sigma/o3756?lang=en&region=US.
30. Higdon, J.J.L. and G.D. Ford, *Permeability of three-dimensional models of fibrous porous media.* Journal of Fluid Mechanics, 1996. 308: p. 341-361.
31. Li, X., D.R. Ballerini, and W. Shen, *A perspective on paper-based microfluidics: Current status and future trends.* Biomicrofluidics, 2012. 6(1): p. 11301-1130113.
32. Righetti, P.G., *Isoelectric focusing : theory, methodology, and applications*. 1st ed. Laboratory techniques in biochemistry and molecular biology. 1983, Amsterdam ; New York New York: Elsevier Biomedical Press ; Sole distributors for the U.S.A. and Canada, Elsevier-North Holland. xv, 386 p.
33. Harden, V.P. and J.O. Harris, *The isoelectric point of bacterial cells.* J Bacteriol, 1953. 65(2): p. 198-202.

APPENDICES

APPENDIX A: PROTOCOLS

A.1 Making Orange G Dye Solutions

Purpose: To make 50 ml of 10 mM and 1 mM Orange G solutions.

Materials:

- Two 50 ml beakers
- Orange G dye powder
- DI water
- Weighing tray
- Scale
- Stir stick

Procedure:

1. Weigh measuring tray and tare scale so that is reads zero.
2. Weigh out 0.226 g of O.G. in measuring tray and place into beaker 1. (Note that gloves and goggles should be worn when handling dye)
3. Weigh out 0.0226 of O.G. in measuring tray and place into beaker 2.
4. Add DI water to each beaker so that the water level reaches 50 ml.
5. Use stir stick to mix solution until all dye has dissolved into water.

A.2 Paper Chip Fabrication Protocol

Purpose: To create paper microfluidic chips that can support electrophoresis.

Materials:

- Whatman 3001-861 Grade 1 Chr Cellulose Chromatography Paper 20 x 20 cm sheets
- AutoCad Drawing of Chip
- Zerox color qube wax printer
- Hot Plate
- Pelco conductive graphite and extender

- Scotch tape
- Scissors
- Letter paper 8.5 x 11 in

Procedure:

1. Connect computer to printer.
2. Open autocad drawing.
3. Try and fit as many duplicates at possible into a 20 x 20 cm area to fit cellulose paper size, if applicable.
4. Switch from “Model view” to “Layout 1” view at the bottom which will switch view to a 8.5 by 11 in paper background.
5. Because the layout unit is inches and the model used cm, the layout view needs to be scaled so that it will print the right size. To set the scale, click to down arrow next to the view scale on the bottom left of the screen.
6. Scroll to the bottom of the drop-down menu and click custom. In the popup box click add. In the box give a name to the scale and set paper units to 0.393701 and drawing units to 1. Click ok and select the new scale in the drop down menu. The drawing should scale to the correct size. (Note: the drawing size should look correct compared to the size of the paper now)
7. While in the correctly scaled layout view, hit the print button in Autocad and in the print setting that pops up before printing click the correct printer and paper size. The scale should be 1 to 1 because the layout was scaled previously.
8. Print drawing onto letter paper and max sure the printer prints to scale check by measuring drawing after print.
9. If correct place cellulose paper over printed letter paper drawing so that printed area is covered.
10. Tape cellulose paper to letter paper be sure to cover all edges.
11. Place paper into printer and print again. (note: paper orientation is critical, and printer will only print correctly in one orientation)

12. The Autocad drawing should have printed onto the cellulose paper now. Remove cellulose paper from letter paper it was attached to.
13. Turn on hot plate and set to 100 C.
14. Once hot, place cellulose paper onto hot plate with printed side up. Wait 30 seconds. Check bottom side of paper to check if wax completely impregnated paper. If not, add back to hot plate,checking periodically to be sure that wax has melted completely through paper.
15. Next cut tape strips so that they are about 4.5 mm in thickness and 1 cm long. Cover electrophoretic zone of channels so that there is just a little bit of non-wax impregnated paper uncovered by the tape and the wax barrier. Tape should protect electrophoretic zone from graphite.
16. Mix colloidal graphite and extender in dish until the consistency is that of paint. Next, using the brush on the lid of the graphite bottle, paint the graphite onto the wax walls, and paint towards the electrophoretic zone until it covers the tap. Do this for both sides.
17. Remove tape. The electrophoretic zone should be uncovered, and clean electrode lines that just barely touch the paper should be present.
18. Let chip dry for an hour.

A.3 Electrophoretic Drift Velocity Measurement Protocol

Purpose: To apply electrophoresis to a paper chip and measure drift velocity with Orange G dye

Materials:

- 50 ml of 1 mM Orange G dye
- 50 ml of 10 mM Orange G dye
- 2 petri dishes
- Glass slide
- 2 alligator clips
- 20 gage wire

- 14 cm long paper chip
- Voltage sequencer
- Camera
- Beaker
- Water
- Paper towels
- Ruler

Protocol:

1. Fill one petri dish with 10 ml of Orange G dye.
2. Fill one petri dish with water.
3. Fill beaker with water.
4. Connect 1 alligator clip to the petri dish with O.G dye and the other alligator clip to the petri dish with water. Be sure that each alligator clip is in contact with the water or the dye.
5. Find the leads on the voltage sequence labeled “A” and add a small piece of 20 gage wire to the positive and negative leads so that about a quarter inch is hanging out.
6. Attach the positive lead to the petri dish with water and the negative lead to the Orange G petri dish. Measure distance between the alligator clip on the petri dish and set them to be 20 cm apart.
7. Place paper chip into beaker with water and remove; pat the chip dry with paper towel so that it does not look like there is any free water.

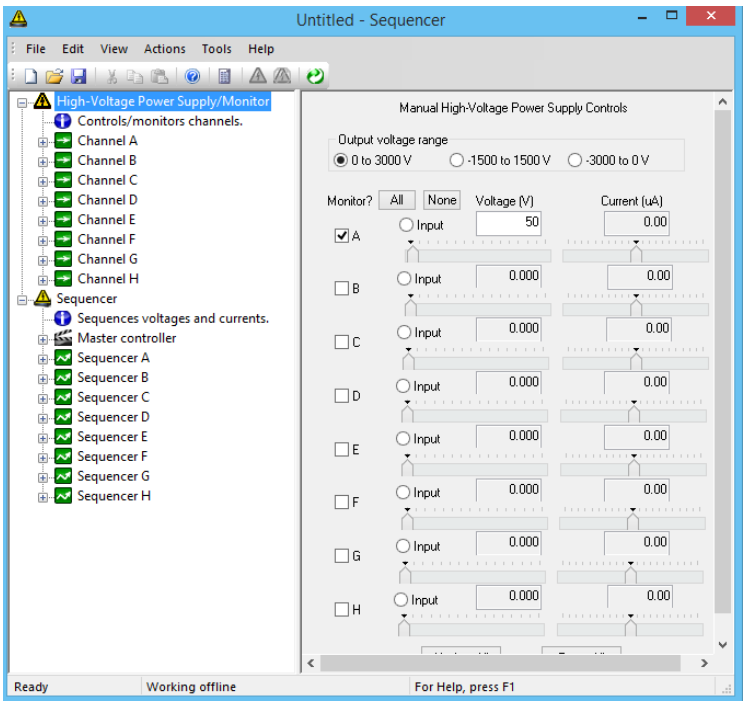

8. Remove tape cover on back of chip and place so that the chip is centered on the glass slide in the long direction and so that the ends of the chip hang equally over the side of the slide.
9. Place slide on the rim of the petri dishes so that it is balanced and centered between the petri dishes. Make sure the paper chip edges that hang over are in contact with the water and the dye solution is forming a bridge between them.
10. Set ruler next to chip so that the start of the ruler lines up with the edge of the glass slide closest to the petri dish with the dye.
11. Open the Labsmith sequence program.
12. Click the high voltage power supply/ monitor box in the left navigation window. Check the monitor box and enter desired voltage in voltage box.
13. Click the green arrow button to connect to the sequencer in the top tool bar on the left side. Once connected, click the yellow triangle with a lightning bolt in it to apply voltage. If connected correctly, the voltage should remain constant, and current should remain relatively constant but my change over time.

14. Set camera above chip and record for so that dye travels farther than 1 cm
15. After the dye reaches 1 cm, click the yellow triangle with a red circle and a line through it to turn off voltage.
16. Save video.
17. Repeat so that 5 experiments of 0, 50, 100, 150, and 200 V are performed.
18. Calculate drift velocity by watching video and subtracting the time from the start of the zero mark on the ruler and the time at one centimeter.

A.4 Paper Microfluidic Chip Separation Protocol

Purpose: To separate Orange G dye into a different channel on a paper microfluidic chip.

Material:

- 50 ml of 1 mM Orange G dye
- 50 ml of 10 mM Orange G dye
- Glass slide
- 2 alligator clips
- 20 gage wire
- paper chip
- Voltage sequencer
- Paper towels

Procedure:

1. Remove tape cover on back of paper chip and stick the paper chip to a glass slide.
2. Connect the alligator clips to the electrodes on the paper chip.
3. Put 20 gage wire into the “A” leads of the voltage sequencer so that a half centimeter sticks out, and connect an alligator clip to each lead.
4. Turn on the voltage sequencer and open the sequencer program.
5. Click tools tab in the toolbar and click simple sequence wizard.

6. For step A change the switch step to “After Delay” and enter 37000 ms and set the next step to “Step B”; then in the channel setting enter required voltage
7. Click Step B on the top toolbar;make sure the switch step is set to only manually and enter the required voltage for step B.
8. Click apply at the bottom and upload to the sequencer.
9. Add one drop of Orange G dye to the application area of the chip.
10. Monitor channel A and once the circuit is completed by the dye touching the electrodes, click “A” in the “Run status.” The sequencer will change automatically to step B after 37 seconds.
11. Once the chip finishes running, click stop.
12. Repeat five times for each dye concentration.

APPENDIX B: CAD DRAWINGS

B.1 Drift Velocity Measuring Strips

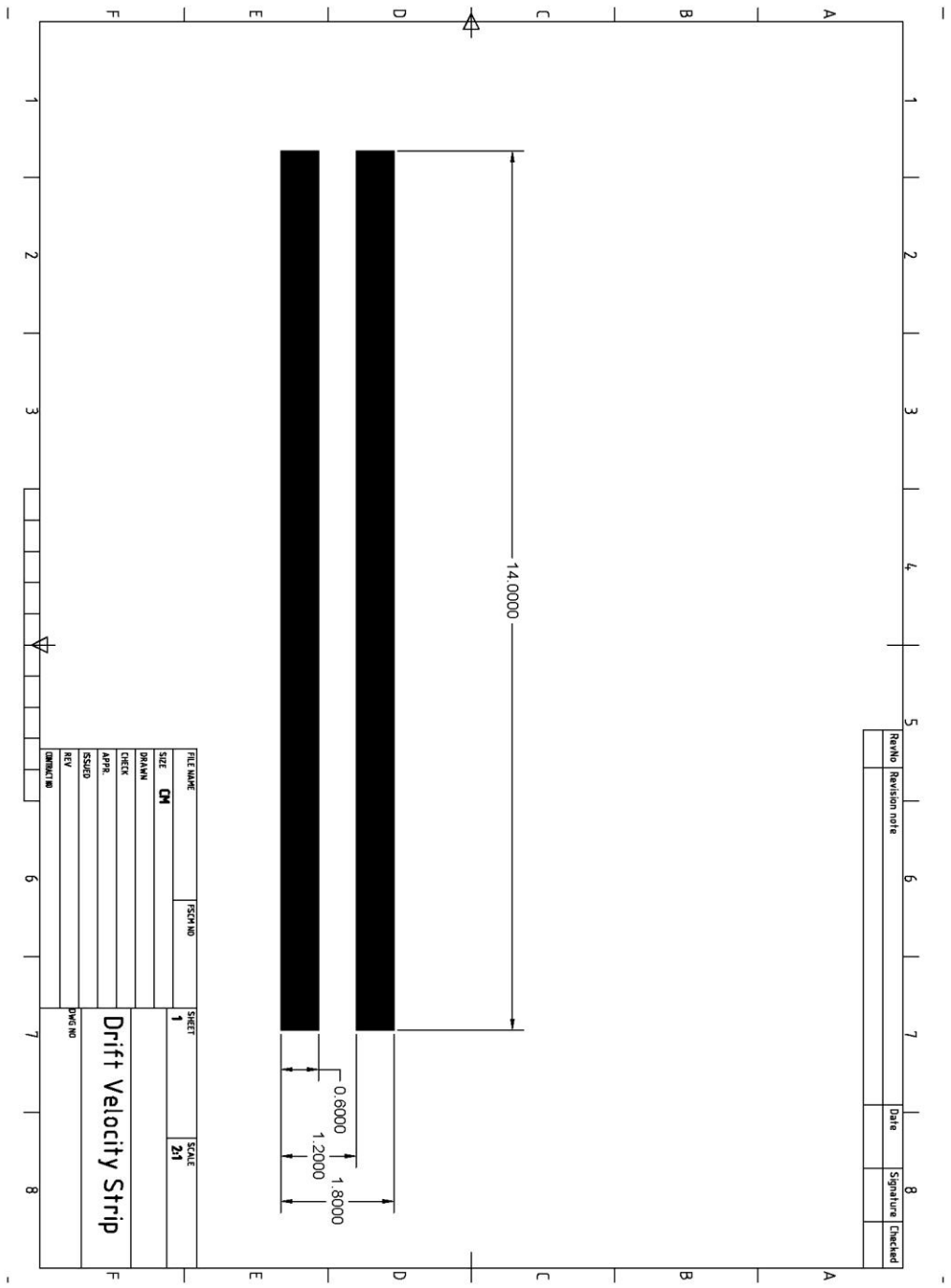

B.2 Electrophoretic Separation Chip

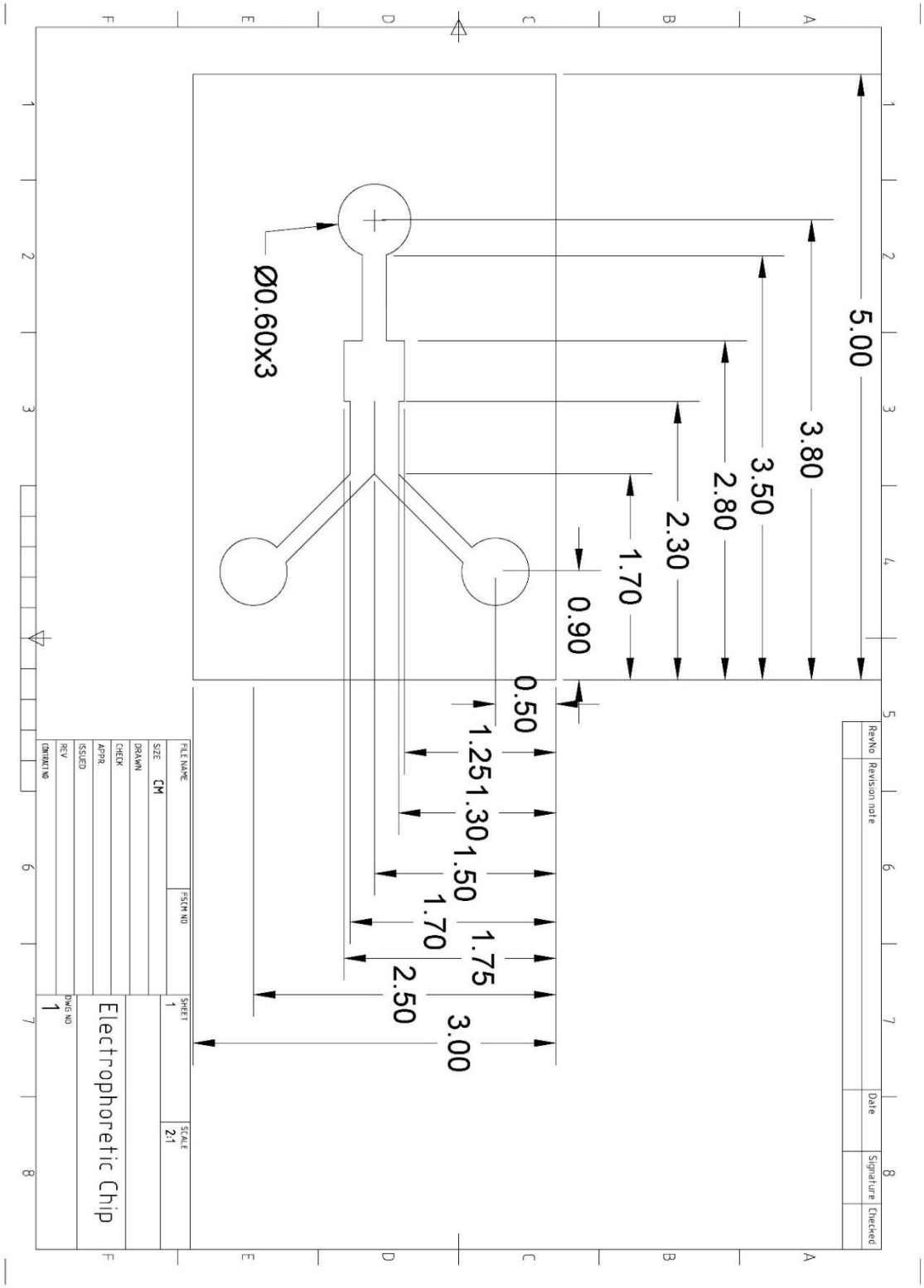
5.00
3.80
3.50
2.80
2.30
1.70
0.90
Ø0.60x3
0.50
1.25
1.30
1.50
1.70
1.75
2.50
3.00
RevNo
Revision note
Date
Signature
Checked
FILE NAME
FSCM NO
SIZE
CM
SHEET
1
SCALE
2:1
DRAWN
CHECK
APPR.
ISSUED
REV
CONTRACT NO
DWG NO
1
Electrophoretic Chip

APPENDIX C: DATA AND STATISTICS

C.1 Electrophoresis Zone Flow Time Data

Dye	Concentration	Time to side wall	Time to run channel
OG	1mM	13.33	53
OG	1mM	14.31	59
OG	1mM	14.88	57.34
OG	1mM	14.38	54
OG	1mM	12.61	55.44
OG	10mM	12.89	50.23
OG	10mM	13.37	61.04
OG	10mM	15.94	56.56
OG	10mM	14.25	60.94
OG	10mM	13.12	59.7

C.2 Drift Velocity Data

Dye	Conc (mM)	Volt (v)	Start Time (sec)	Finish Time (sec)	Distance (mm)	Velocity (mm/min)	Normalized Velocity (mm/min)
O.G.	10	0	83	574	10	1.222	
O.G.	10	0	100	670	10	1.053	
O.G.	10	0	81	627	10	1.099	
O.G.	10	0	84	694	10	0.984	
O.G.	10	0	212	857	10	0.930	
O.G.	10	50	53	408	10	1.690	0.633
O.G.	10	50	163	554	10	1.535	0.477
O.G.	10	50	64	440	10	1.596	0.538
O.G.	10	50	79	478	10	1.504	0.446
O.G.	10	50	24	331	10	1.954	0.897

O.G.	10	100	78	300	10	2.703	1.645
O.G.	10	100	61	315	10	2.362	1.305
O.G.	10	100	22	267	10	2.449	1.392
O.G.	10	100	94	370	10	2.174	1.116
O.G.	10	100	28	265	10	2.532	1.474
O.G.	10	150	54	262	10	2.885	1.827
O.G.	10	150	41	261	10	2.727	1.670
O.G.	10	150	91	345	10	2.362	1.305
O.G.	10	150	15	203	10	3.191	2.134
O.G.	10	150	64	259	10	3.077	2.019
O.G.	10	200	30	185	10	3.871	2.813
O.G.	10	200	56	235	10	3.352	2.294
O.G.	10	200	62	239	10	3.390	2.332
O.G.	10	200	51	218	10	3.593	2.535
O.G.	10	200	97	276	10	3.352	2.294
O.G.	1	0	152	760	10	0.987	
O.G.	1	0	124	744	10	0.968	
O.G.	1	0	368	921	10	1.085	
O.G.	1	0	226	853	10	0.957	
O.G.	1	0	248	790	10	1.107	
O.G.	1	50	42	394	10	1.705	0.684
O.G.	1	50	30	383	10	1.700	0.679
O.G.	1	50	140	540	10	1.500	0.479
O.G.	1	50	115	525	10	1.463	0.443
O.G.	1	50	54	429	10	1.600	0.579
O.G.	1	100	22	288	10	2.256	1.235
O.G.	1	100	69	383	10	1.911	0.890
O.G.	1	100	48	337	10	2.076	1.055
O.G.	1	100	11	304	10	2.048	1.027

O.G.	1	100	39	282	10	2.469	1.448
O.G.	1	150	103	301	10	3.030	2.010
O.G.	1	150	125	363	10	2.521	1.500
O.G.	1	150	168	405	10	2.532	1.511
O.G.	1	150	83	335	10	2.381	1.360
O.G.	1	150	127	369	10	2.479	1.459
O.G.	1	200	464	660	10	3.061	2.041
O.G.	1	200	79	246	10	3.593	2.572
O.G.	1	200	107	305	10	3.030	2.010
O.G.	1	200	135	304	10	3.550	2.530
O.G.	1	200	79	288	10	2.871	1.850

C.3 Drift Velocity Statistics

One-way ANOVA: 10 mM versus Voltages

```
Source    DF     SS     MS     F     P
Voltages   3  9.0388  3.0129  52.98  0.000
Error     16  0.9099  0.0569
Total     19  9.9486
S = 0.2385   R-Sq = 90.85%   R-Sq(adj) = 89.14%

                    Individual 95% CIs For Mean Based on
                    Pooled StDev
Level  N    Mean   StDev  ----+---------+---------+---------+-----
 50    5  0.5982  0.1815  (---*---)
100    5  1.3864  0.1964            (---*---)
150    5  1.7910  0.3249                  (---*---)
200    5  2.4540  0.2245                        (---*---)
                  ----+---------+---------+---------+-----
                   0.60      1.20      1.80      2.40
Pooled StDev = 0.2385
```

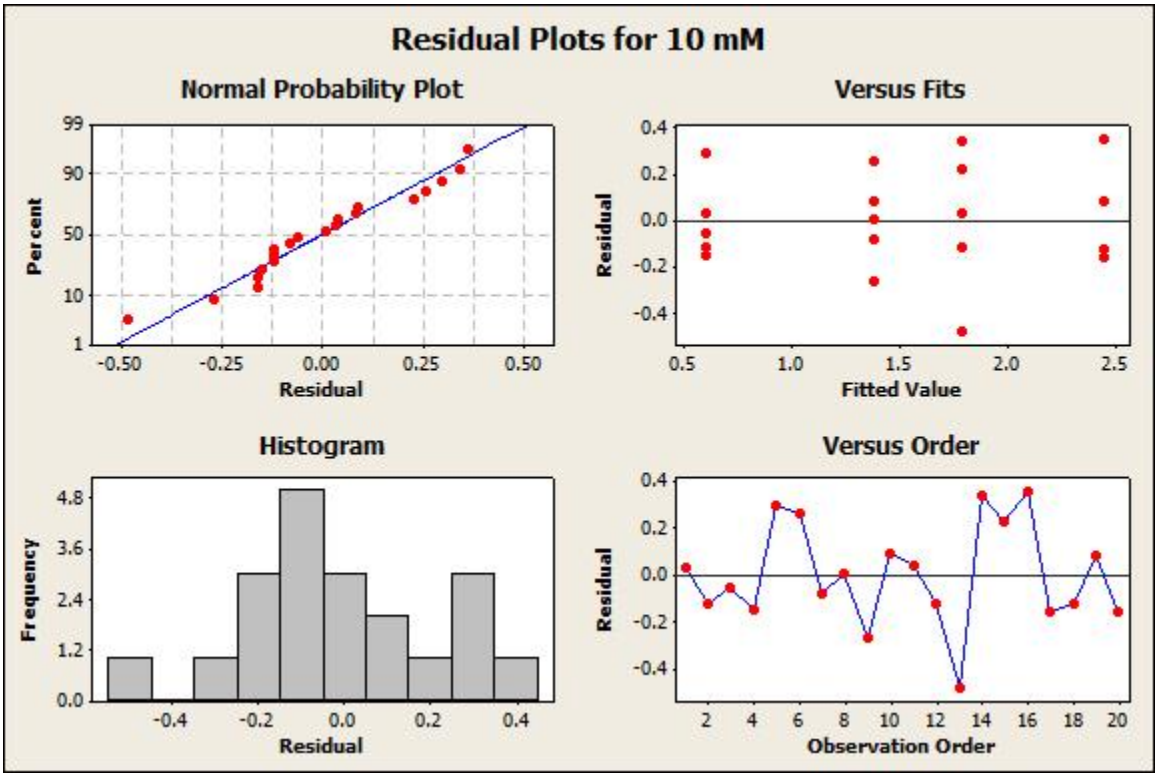

Because P<0.05 there is at least one voltage that is significantly different. To used T-Test to compare each voltage pair.

Two-Sample T-Test and CI: 10 mM O.G. 50 V Vs100 V

Two-sample T for C8

C9 N Mean StDev SE Mean

50 5 0.598 0.182 0.081

100 5 1.386 0.196 0.088

Difference = mu (50) - mu (100)

Estimate for difference: -0.788

95% CI for difference: (-1.071, -0.505)

T-Test of difference = 0 (vs not =): T-Value = -6.59 P-Value = 0.000 DF = 7

Two-Sample T-Test and CI: 10 mM O.G. 100 V Vs150 V

Two-sample T for C10

C11 N Mean StDev SE Mean

100 5 1.386 0.196 0.088

150 5 1.791 0.325 0.15

Difference = mu (100) - mu (150)

Estimate for difference: -0.405

95% CI for difference: (-0.820, 0.011)

T-Test of difference = 0 (vs not =): T-Value = -2.38 P-Value = 0.055 DF = 6

P>0.05 with P=0.055, P is barely no significant.

Two-Sample T-Test and CI: 10 mM O.G. 150 V Vs200 V

Two-sample T for C12

C13	N	Mean	StDev	SE Mean
150	5	1.791	0.325	0.15
200	5	2.454	0.224	0.10

Difference = mu (150) - mu (200)

Estimate for difference: -0.663

95% CI for difference: (-1.081, -0.245)

T-Test of difference = 0 (vs not =): T-Value = -3.75 P-Value = 0.007 DF = 7

One-way ANOVA: 1 mM O.G. versus the Voltages

Source	DF	SS	MS	F	P
C6	3	7.1061	2.3687	40.99	0.000
Error	16	0.9246	0.0578		
Total	19	8.0307			

S = 0.2404 R-Sq = 88.49% R-Sq(adj) = 86.33%

Individual 95% CIs For Mean Based on Pooled StDev

Level	N	Mean	StDev	----+---------+---------+---------+-----
50	5	0.5728	0.1110	(---*--)
100	5	1.1312	0.2157	(---*---)
150	5	1.5679	0.2540	(---*---)
200	5	2.2004	0.3283	(---*--)

----+---------+---------+---------+-----

0.60 1.20 1.80 2.40

Pooled StDev = 0.2404

Because P<0.05 there is at least one voltage that is significantly different. To used T-Test to compare each voltage pair.

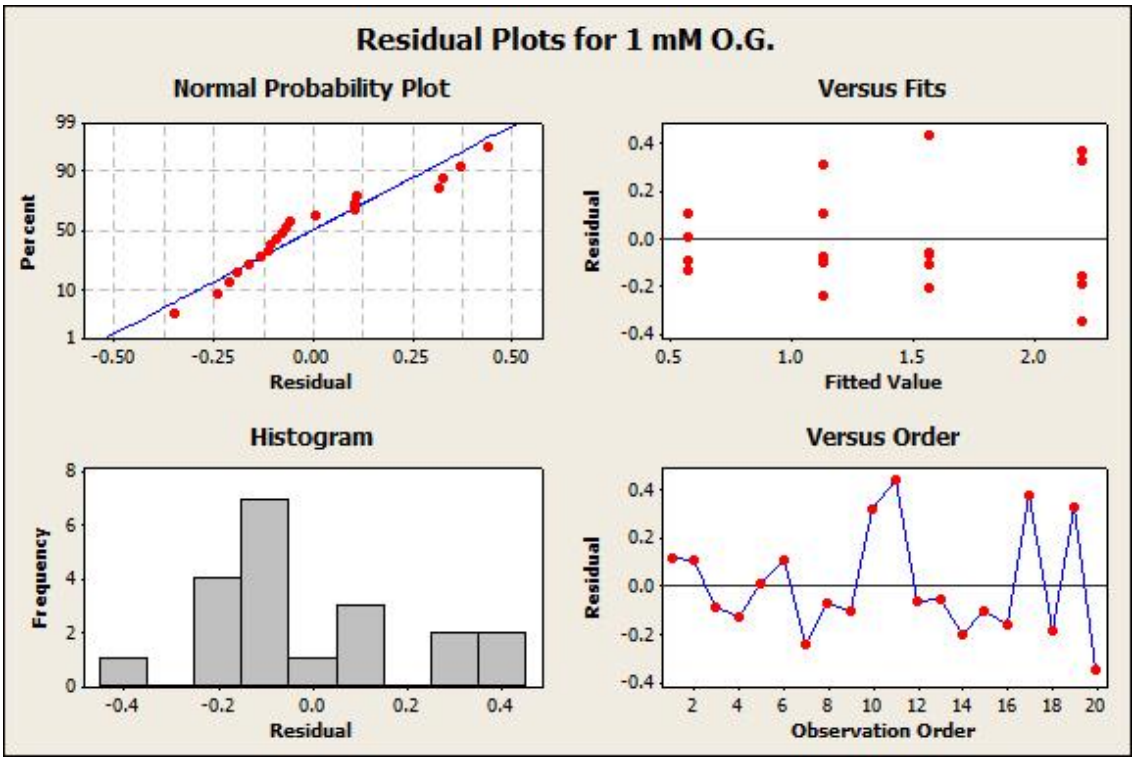

Two-Sample T-Test and CI: 1 mM O.G. 50 V Vs 100 V

Two-sample T for C31

C32 N Mean StDev SE Mean

50 5 0.573 0.111 0.050

100 5 1.131 0.216 0.096

Difference = mu (50) - mu (100)

Estimate for difference: -0.558

95% CI for difference: (-0.809, -0.308)

T-Test of difference = 0 (vs not =): T-Value = -5.15 P-Value = 0.001 DF = 8

Both use Pooled StDev = 0.1715

Two-Sample T-Test and CI: 1 mM O.G. 100 V Vs 150 V

Two-sample T for C28

C29 N Mean StDev SE Mean

100 5 1.131 0.216 0.096

150 5 1.568 0.254 0.11

Difference = mu (100) - mu (150)

Estimate for difference: -0.437

95% CI for difference: (-0.780, -0.093)

T-Test of difference = 0 (vs not =): T-Value = -2.93 P-Value = 0.019 DF = 8

Both use Pooled StDev = 0.2356

Two-Sample T-Test and CI: 1 mM O.G. 150 V Vs 200 V

Two-sample T for C34

C35 N Mean StDev SE Mean

150 5 1.568 0.254 0.11

200 5 2.200 0.328 0.15

Difference = mu (150) - mu (200)

Estimate for difference: -0.632

95% CI for difference: (-1.061, -0.204)

T-Test of difference = 0 (vs not =): T-Value = -3.41 P-Value = 0.009 DF = 8

Both use Pooled StDev = 0.2935

Two-Sample T-Test and CI: 10 mM vs 1 mM at 50 V

Two-sample T for C16 vs C17

N Mean StDev SE Mean

C16 5 0.598 0.182 0.081

C17 5 0.573 0.111 0.050

Difference = mu (C16) - mu (C17)

Estimate for difference: 0.0254

95% CI for difference: (-0.2074, 0.2582)

T-Test of difference = 0 (vs not =): T-Value = 0.27 P-Value = 0.798 DF = 6

Two-Sample T-Test and CI: 10 mM vs 1 mM at 100 V

Two-sample T for C19 vs C20

N Mean StDev SE Mean

C19 5 1.386 0.196 0.088

C20 5 1.131 0.216 0.096

Difference = mu (C19) - mu (C20)

Estimate for difference: 0.255

95% CI for difference: (-0.053, 0.564)

T-Test of difference = 0 (vs not =): T-Value = 1.96 P-Value = 0.091 DF = 7

Two-Sample T-Test and CI: 10 mM vs 1 mM at 150 V

Two-sample T for C22 vs C23

N Mean StDev SE Mean

C22 5 1.791 0.325 0.15

C23 5 1.568 0.254 0.11

Difference = mu (C22) - mu (C23)

Estimate for difference: 0.223

95% CI for difference: (-0.213, 0.659)

T-Test of difference = 0 (vs not =): T-Value = 1.21 P-Value = 0.266 DF = 7

Two-Sample T-Test and CI: 10 mM vs 1 mM at 200 V

Two-sample T for C25 vs C26

	N	Mean	StDev	SE Mean
C25	5	2.454	0.224	0.10
C26	5	2.200	0.328	0.15

Difference = mu (C25) - mu (C26)

Estimate for difference: 0.254

95% CI for difference: (-0.167, 0.674)

T-Test of difference = 0 (vs not =): T-Value = 1.43 P-Value = 0.197 DF = 7

Regression Analysis: Normal 10 mM versus Electric Field

The regression equation is

Normal 10 mM = 0.064 + 0.00239 Electric Field

Predictor	Coef	SE Coef	T	P
Constant	0.0644	0.1356	0.48	0.682
Electric Field	0.0023888	0.0001981	12.06	0.007

S = 0.110730 R-Sq = 98.6% R-Sq(adj) = 98.0%

Analysis of Variance

Source	DF	SS	MS	F	P
Regression	1	1.7832	1.7832	145.44	0.007
Residual Error	2	0.0245	0.0123		
Total	3	1.8078			

Regression Analysis: Normal 1 mM versus Electric Field

The regression equation is

Normal 1 mM = 0.0382 + 0.00213 Electric Field

Predictor	Coef	SE Coef	T	P
Constant	0.03824	0.06931	0.55	0.637
Electric Field	0.0021278	0.0001012	21.02	0.002

S = 0.0565954 R-Sq = 99.5% R-Sq(adj) = 99.3%

Analysis of Variance

Source	DF	SS	MS	F	P
Regression	1	1.4148	1.4148	441.71	0.002
Residual Error	2	0.0064	0.0032		
Total	3	1.4212			

C.4 Orange G Separation Trace Graphs

1mM Traces Trial 1

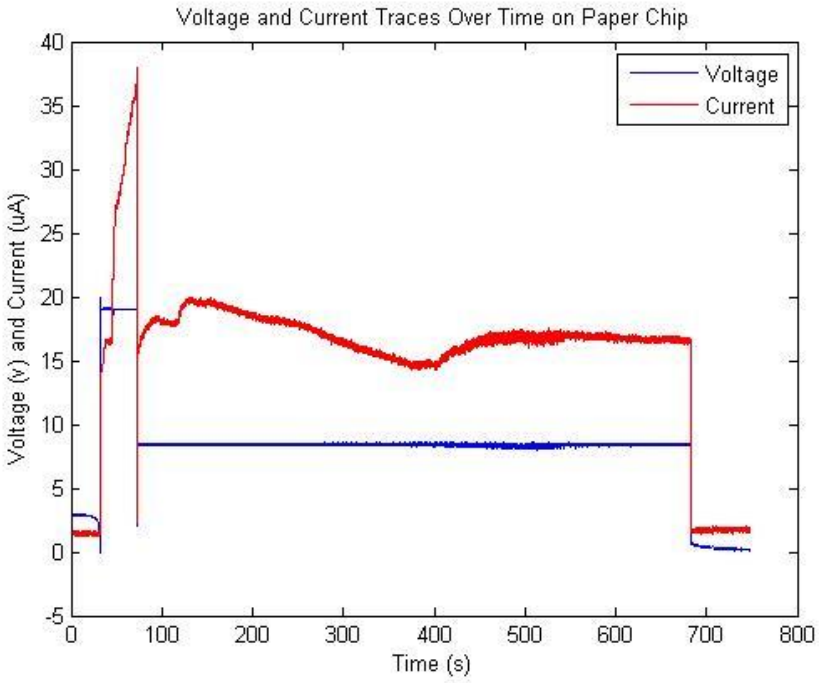

1mM Traces Trial 2

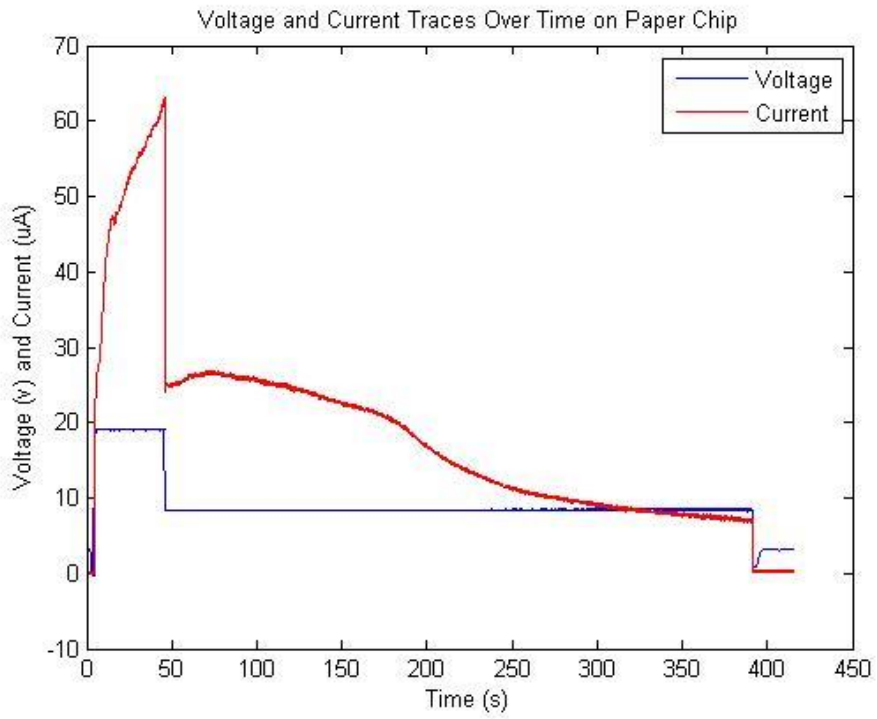

1mM Traces Trial 3

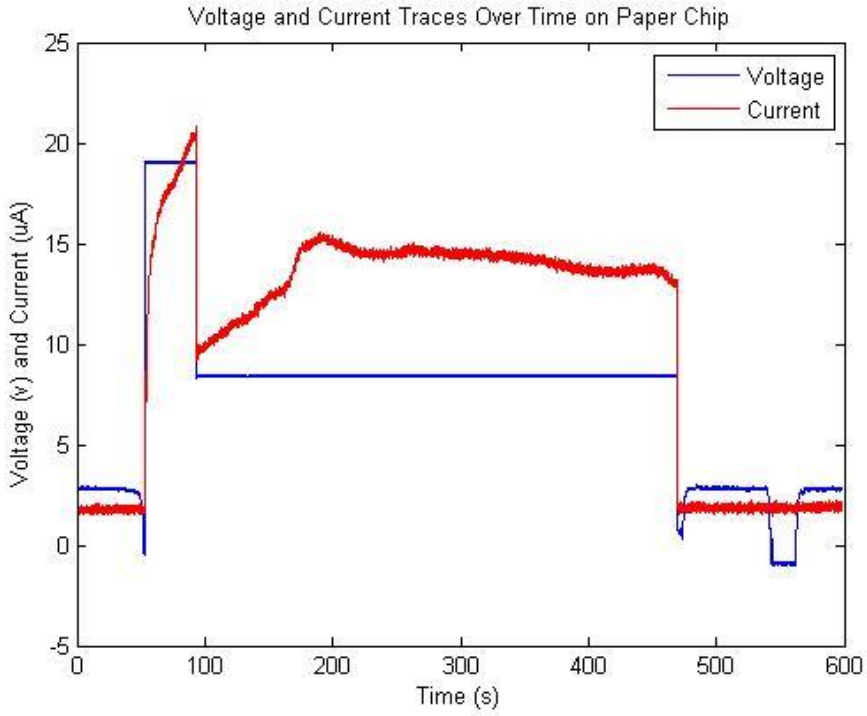

1mM Traces Trial 4

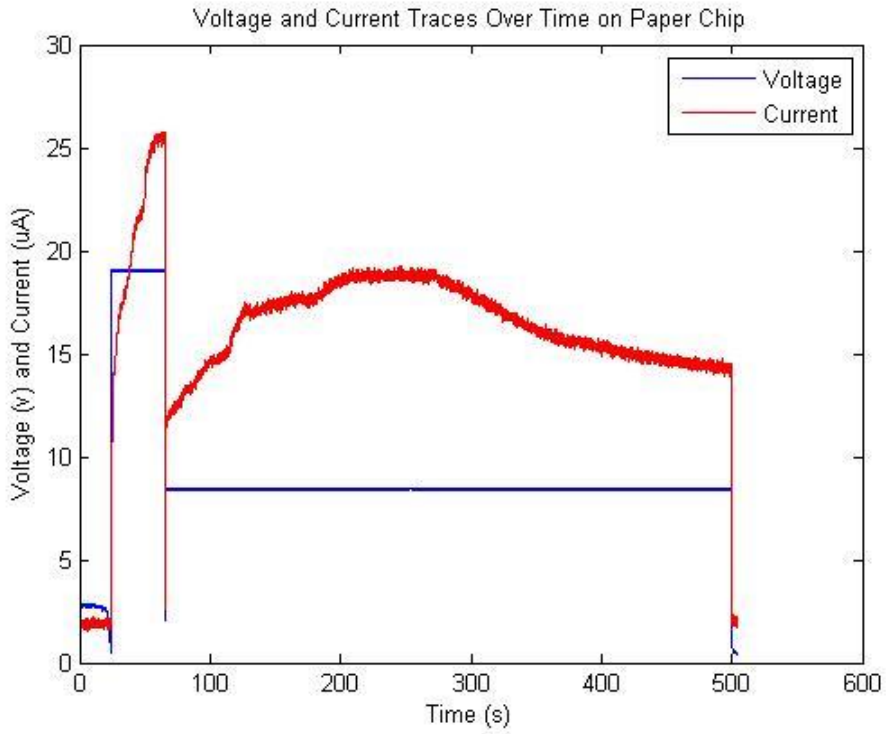

1mM Traces Trial 5

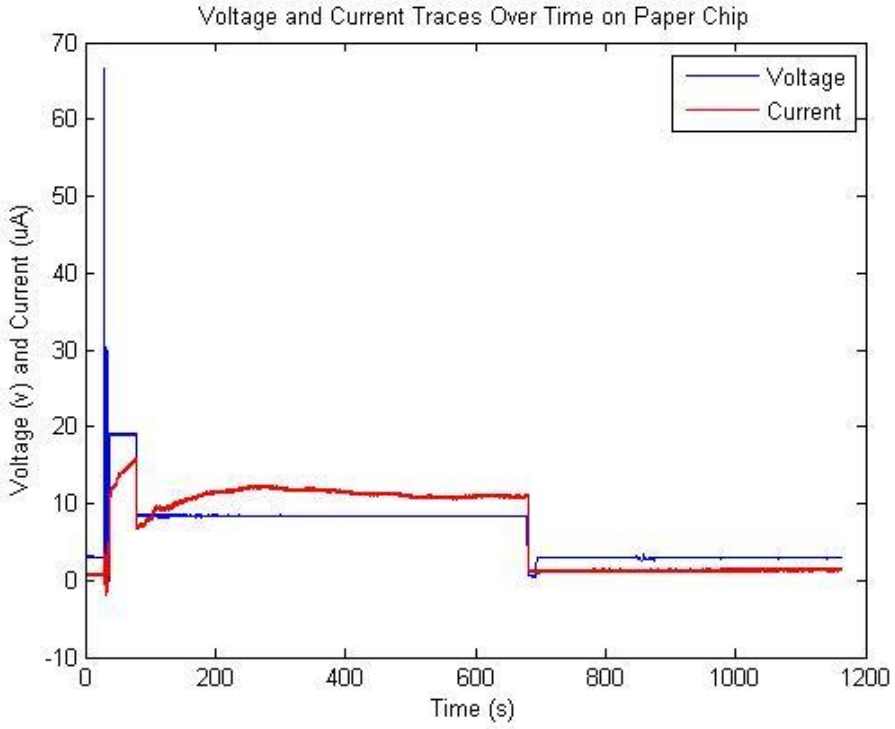

1mM Traces Trial 6

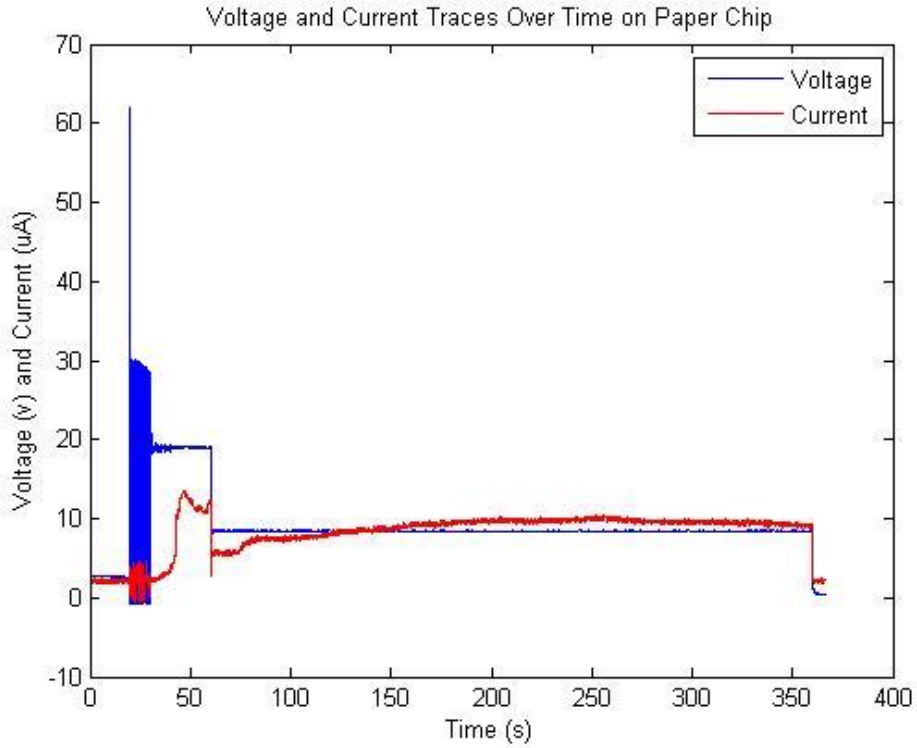

1mM Traces Trial 1

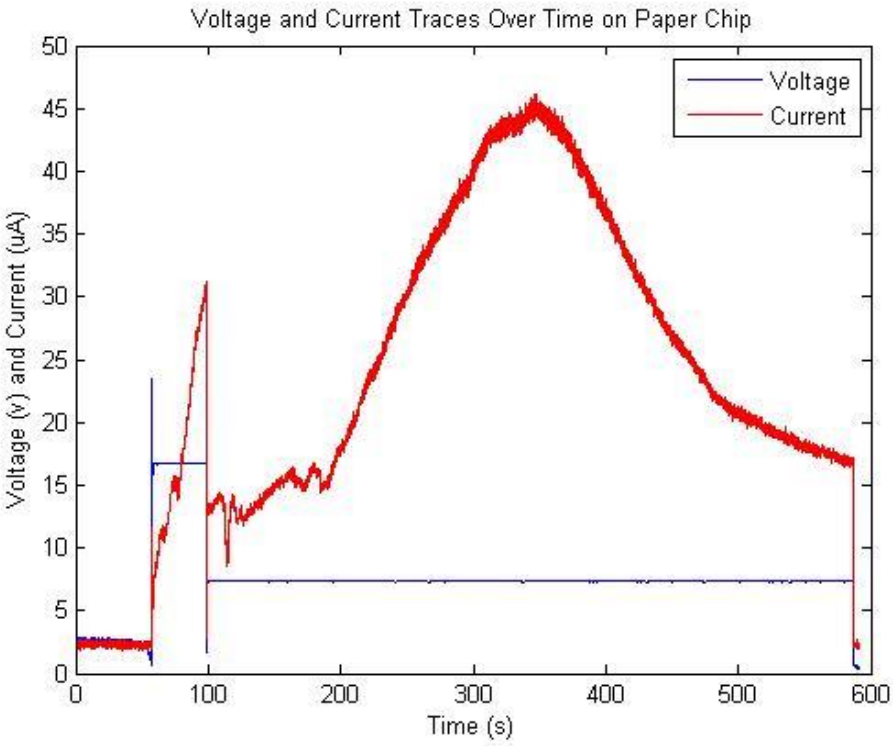

1mM Traces Trial 2